Università degli Studi di Milano
Department of Biomedical Sciences for Health
PhD course in Integrated Biomedical Research
XXXII cycle

PhD thesis

Optimisation of contrast agent administration for CT and MRI

PhD thesis by:
Moreno Zanardo
R11689

Advisor: Prof. Francesco SARDANELLI

Contents

Abbreviations

AGD: average glandular dose

ALCE: adjusted liver contrast enhancement

ANOVA: analysis of variance

BMI: body mass index

CC: craniocaudal

CE-MRA: contrast enhanced magnetic resonance angiography

CENTRA: contrast-enhanced timing robust angiography

CESM: contrast-enhanced spectral mammography

CHD: congenital heart diseases

CoV: coefficient of variation

CT: computed tomography

FA: flip angle

FOV: field of view

GBCA: gadolinium-based contrast agent

gI: grams of iodine

GRAPPA: generalized autocalibrating partial parallel acquisition

HU: hounsfield units

ICM: iodinated contrast medium

IQR: interquartile range

LBW: lean body weight

LCE: liver contrast enhancement

MLO: mediolateral oblique

MRI: magnetic resonance imaging

NSF: nephrogenic systemic fibrosis

PRISMA: preferred reporting items for systematic reviews and meta-analyses

SD: standard deviation

SENSE: sensitivity encoding

TBW: total body weight

TE: echo time

TR: repetition time

TRICKS: time-resolved imaging of contrast kinetics

TR-MRA: time-resolved magnetic resonance angiography

TWIST: time-resolved angiography with stochastic trajectories

Summary

During the PhD course my research projects focused mainly on the effectiveness, safety and optimisation of contrast agents in computed tomography (CT) and magnetic resonance imaging (MRI), subdivided into different studies. This doctoral thesis aims at explore the possible optimisation of contrast medium administration protocols in different clinical contexts.

In the first section of my thesis, we proposed two studies focused on the optimisation of the practice of iodinated contrast medium (ICM) injection in CT. First, we tried to verify the conditions for a change in the dose calculation to be administered in patients undergoing an abdominal CT. Since decades, it is an established practice to inject a dose of ICM calculated on the patient total body weight (TBW). However, this approach does not consider the different volume of biodistribution among patients with different body mass index (BMI). Indeed, it was demonstrated that the ICM poorly distributes in adipose tissue and obese patients may receive a higher dose than that really needed. We have hypothesized that dosing ICM as based on the lean body weight (LBW) would be a more appropriate approach. We firstly retrospectively calculated an ICM dose based on LBW that was equivalent to the dose based on TBW in terms of liver contrast enhancement (LCE). We found that the injected ICM dose was highly variable, with underweight patients receiving a higher dose than obese patients, as a radiologist-driven compensation effect.

Starting from the results obtained from the retrospective study, we conducted a randomized controlled trial based on the dose equivalent between the ICM based on patient TBW and the dose calculated using LBW. The Ethics Committee approved the single-center, double-blinded randomized controlled trial (trial registration NCT03384979). Patients were randomized to LBW-based ICM dose (0.61 gI/kg of lean body weight), or TBW-based ICM dose (0.44 gI/kg of TBW) and these equivalent doses derived from the retrospective study. In conclusion, LBW- and TBW-based ICM doses lead to a similar LCE with no significantly different variation for the LBW group, negating the study hypothesis and highlighting the knowledge gap about factors affecting LCE.

The last part of the section I aimed to systematically review contrast-enhanced spectral mammography (CESM) studies, focusing on adopted CESM technique, ICM issues and adverse reactions ICM related. Of 120 retrieved articles, 84 were included, totalling 14,012 patients. Contrast type and concentration was reported in 79/84 studies (94%), with Iohexol 350 mgI/mL mostly used (25/79, 32%), dose and flow rate in 72/84 (86%), with 1.5 mL/kg dose at 3 mL/s in 62/72 studies (86%). Thirty adverse reactions were reported by 14/84 (17%) studies (26 mild, 3 moderate, 1 severe non-fatal) with a pooled rate of 0.82%. Factory-set kVp, contrast 1.5-mL/kg at 3 mL/s, and 120-s acquisition delay were mostly used and only 1 severe adverse reaction was reported.

In the second PhD thesis section, I focused on gadolinium-based contrast agent (GBCA) protocol issues. A systematic review was conducted in collaboration with the University College Dublin (Dublin, Ireland) during the six months fellowship and it was regarding GBCA administration protocols used for cardiothoracic applications of time-resolved (TR) magnetic resonance angiography (MRA) sequences. A search of the literature was performed to identify articles utilising TR-MRA sequences, focusing on type of sequence, adopted technical parameters, GBCA issues and acquisition workflow. Of 117 retrieved articles, 16 matched the inclusion criteria and study population ranged from 5 to 185 patients, for a total of 506 patients who underwent cardiothoracic TR-MRA. The administered GBCA was gadobutrol (Gadovist) in 6/16 (38%) articles, gadopentetate dimeglumine (Magnevist) in 5/16 (31%), gadobenate dimeglumine (Multihance) in 2/16 (13%), gadodiamide (Omniscan) in 2/16 (13%), gadofosveset trisodium (AblavarTM) in 1/16 (6%). GBCA showed highly variable doses among studies: fixed amount or based on patient body weight (0.02–0.2 mmol/kg). In conclusions, a consensus on technique for cardiothoracic applications of TR-MRA is still far from reached, mostly due to differences regarding contrast agent type and dose. Further studies are warranted to provide a common standardised acquisition protocol.

SECTION I: IODINATED-BASED CONTRAST MEDIUM

This section is based on:

- *Zanardo et al. Abdominal CT: a radiologist-driven adjustment of the dose of iodinated contrast agent approaches a calculation per lean body weight. Eur Radiol Exp. 2018;2(1):41.*
- *Zanardo et al. Using the lean body weight (LBW) instead of total body weight (TBW) to dose the iodinated contrast agent for abdominal CT: a randomized controlled trial. Under revision on Radiology.*
- *Zanardo et al. Technique, protocols, and adverse reactions for contrast-enhanced spectral mammography (CESM): a systematic review. Insight into Imaging. Doi: 10.1186/s13244-019-0756-0*

Introduction

In the current clinical context, where the strive to achieve personalised, precision medicine has become increasingly important, research on ICM dose optimisation is assuming a crucial role (1,2). Individual, morphometric-tailored dose approaches for ICMs have become more common in recent years. This is paving the way to make personalized ICM administration more concrete and feasible (1,3).

Iodine concentration, injection rate, scanning delay time, saline solution flushing, patient blood pressure and cardiac function are all features affecting the contrast-enhancement in computed tomography (CT) (4–6). When quantitatively assessing the effectiveness of ICMs, liver contrast-enhancement (LCE), being relating to the overall magnitude of enhancement, can be taken as a reference (7). LCE in CT is strongly influenced by the ICM biodistribution into the intra- and extra-vascular space, which are both related to body size (8,9). In fact, in a radiological setting, it is widely accepted that a larger patient needs a higher iodine load to achieve the same magnitude of tissue enhancement compared to a smaller patient. For this reason, it is commonly recognized that dosing ICM on patient total body weight (TBW) instead of using a fixed amount, which however is still a part of usual practice (10), can be more accurate and patient-tailored (11–17).

Is well known that adipose tissue is poorly perfused; as a consequence, ICM poorly distributes fatty body components (5,13,18,19) it is well perfused in lean body weight (LBW) (20,21). Thus, while dosing according to TBW is rationally effective and represents a validated approximation, in patients with different body composition and different proportions between LBW over TBW (e.g., athletes versus obese people), TBW-based dosage could lead to overdosing or underdosing the drug.

Several studies have demonstrated that dosing ICM basing on LBW rather than TBW could lead a better visualization of specific organs, blood vessels or tissues, as well as lesions or tissue anomalies (19,22–30). LBW can be easily determined through a scale equipped with bioelectrical impedance analysis (31), although a formula based on patient TBW, height, and gender is also suitable for its calculation for ICM doses related purposes (21,32,33).

Previous studies using LBW for ICM dose calculation mainly compared different strategies and, to our knowledge, no study has performed an optimisation process to find out what is the minimal diagnostic ICM dose based on the LBW (22–30). Moreover, authors limited their studies mainly to normal weight or overweight populations. In our opinion, advantages of ICM dose calculation based on the LBW instead of the TBW may appear mostly in underweight and obese patients.

Patients with impaired kidney function should be given special consideration before receiving iodinated ICM by vein and especially artery access. Such patients are at risk for developing contrast-induced nephropathy, a condition in which already-impaired kidney function worsens within a few days of contrast material administration (34). Moreover, considering that the administration of iodinated ICM significantly increases radiation-induced DNA damage in blood lymphocytes and a lower ICM iodine dose results in a reduced level of DNA damage, at constant radiation exposure (35), an attempt to reduce ICM is advisable, trying to maintain a sufficient diagnostic quality.

In 1995, Heiken et al. (7) proposed 50 Hounsfield unit (HU) increase of LCE as threshold for a high diagnostic quality abdominal CT, but, to our knowledge, no study has performed an optimisation process to find out an updated threshold considering the technical CT improvement, or based on ICM dosed on LBW.

The aim of this preliminary retrospective study was to report on our experience on multiphasic abdominal CT and to calculate the LBW-derived CA dose that was equivalent to that derived from TBW, leading to the same amount of injected iodine. In other words, our final aim was to find a feasible formula to standardize the amount of liver enhancement across patients of all sizes, whereas the amount of iodine delivered will vary by patient size and by whether lean body weight or total body weight is used to determine the total amount of injected iodine.

Subsequently, our hypothesis was that dosing ICM on the basis of LBW instead of TBW could reduce the chance of overdosing obese patients, as well as to underdosing underweight patients with the overall net effect of reducing the among-patient variability of liver CE and the CE

of other anatomical structures. The aim of this study was to verify this hypothesis in a randomized controlled trial (RCT).

1. Abdominal CT: a radiologist-driven adjustment of the dose of iodinated contrast medium approaches a calculation per lean body weight

Materials and methods LBW retrospective study

Study design and population

This retrospective cross-sectional study was approved by the local Ethics Committee (San Raffaele Hospital, Milan, authorization number 160/int/2016). A series of 201 consecutive patients who underwent a contrast-enhanced multiphasic abdominal CT or portal venous phase CT at our institution from June to September 2016 were reviewed.

Exclusion criteria were: history of chronic liver disease (cirrhosis, local or diffuse liver fatty infiltration, or glycogen storage disease); congestive heart failure; prior cardiac valve replacement; restrictive and/or constrictive pericarditis; implanted devices (pacemakers, defibrillators, insulin pumps). Although Hamer et al. (36) defined steatotic hepatitis when liver parenchyma has an average CT values on unenhanced images lower than 40 HU, we excluded patients with CT values below 30 HU in the unenhanced scan. As a consequence, low grade of steatosis has been presumably included in our study population.

CT protocol

All patients were studied using a 64-row CT scan (Somatom Definition, Siemens Medical Solution, Erlangen, Germany) with 120 kVp, tube load from 100 to 200 mAs depending on automatic exposure control system (CARE Dose 4D, Siemens Medical Solution, Erlangen, Germany), rotation time 0.5 s, pitch 1, B30f medium smooth for kernel reconstruction technique and abdomen window.

Patients TBW and height were registered in an electronic database. Moreover, a radiologist-driven dose of iopamidol (190 patients over 201) (Iopamiro 370; 370 mgI/mL; Bracco Imaging, Milan, Italy) or iomeprol (11 patients over 201) (Iomeron 400; 400 mgI/mL; Bracco Imaging, Milan, Italy) were administered. While iopamidol is the main choice in our hospital for routine abdomen and

chest CT, iomeprol is used for cardiac CT. Due to practical reasons (storage lack of iopamidol, necessity of employ ICM bottle already opened, examination acquired during a cardiac session) some patients received iomeprol. A total of eight radiologists were responsible for the examinations. The general rule established in the department for the ICM dose to be administered for multiphasic abdominal CT was to use doses proportional to the TBW, multiplying the patient body weight by a constant, which varied from 1.1 to 1.3 mL/kg, with adjustments when the ICM dose was considered too high. Radiologists usually adopted their own spontaneous threshold, without any agreement among them. Another heuristic rule used by some professionals was "patient weight in mL plus 10 additional mL of ICM".

The ICM was administered intravenously through a 20-gauge needle using an automatic power injector (EmpowerCTA® Contrast Injection System, Bracco Imaging, Milan, Italy) at the rate of 3 mL/s, followed by 50 mL of saline solution at the same rate.

The scan delay was determined using an automated triggering hardware and a dedicated software (Bolus Tracking, Siemens Medical Solution, Erlangen, Germany). Specifically, low-dose monitor images were obtained in a single axial slice of the aorta after ICM injection. When the descending aorta enhanced more than 100 HU, diagnostic scans of the abdomen were acquired after an additional delay of about 18 s (arterial phase), 30 s after arterial phase (portal venous phase), and, only in specific cases, 90 s (nephrogenic phase). For the aim of this study, we considered only the portal venous phase.

LBW estimation and image analysis

According to the international classification of BMI from the WHO (37), patients were considered underweight when the BMI was lower than 18.5 kg/m^2, normal weighted when between 18.5 kg/m^2 and 25 kg/m^2, overweight when between 25 kg/m^2 and 30 kg/m^2, and obese when higher than 30 kg/m^2.

According to Awai and colleagues (38) and Nyman (32), LBW was calculated using the James formula (39) (**Equation 1**) or the Boer formula (40) (**Equation 2**), due to better adherence of non-obese patients to the first and of obese patients to the latter.

(Equation 1) $$LBW_{James} = \begin{Bmatrix} 1.1 \times weight\ (kg) - 128\ \times \left(\frac{weight\ (kg)}{height\ (m)}\right)^2 men \\ 1.07 \times weight\ (kg) - 148\ \times \left(\frac{weight\ (kg)}{height\ (m)}\right)^2 women \end{Bmatrix}$$

(Equation 2) $$LBW_{Boer} = \begin{Bmatrix} 0.407\ \times weight\ (kg) + 0.267\ \times height - 19.2\, men \\ 0.252\ \times weight\ (kg) + 0.473\ \times height - 48.3\, women \end{Bmatrix}$$

All images were reviewed by a radiology resident with two years of experience in the field of abdominal CT. Attenuation measurements were obtained by manually placing a rounded region of interest in the anterior (III or IVb Couinaud) and in the posterior (VI Couinaud) segments at the level of the main portal vein with a diameter between 2 and 3 cm; these two values were averaged. Two different regions in anterior and posterior liver parenchyma were chosen because of subtle territorial differences in liver enhancement probably due to different level of fatty infiltration and vascularity. Focal hepatic lesions, blood vessels, bile ducts, calcifications, as well as artefacts, if present, were carefully avoided.

Statistical analysis

For each patient, we retrieved from the radiological report the amount and type of injected ICM in mL and the dose was calculated both per TBW and LBW. Moreover, to account for the different concentration of iodine of the two used ICMs, we converted the absolute injected amount from mL to grams of iodine (gI).

The LCE was calculated as the difference between the CT value measured in the portal venous phase and that measured before ICM injection. To this aim, regions of interest were copy-pasted from one phase to another. The distribution of LCE was calculated for the whole population and for the four subgroups of BMI. Bivariate correlation analysis was performed using the Pearson correlation coefficient. The comparison of the mean ICM dose as well as of the mean LCE among the four

subgroups of BMI was performed using the one-way analysis of variance (ANOVA); the variance of LCE was compared using the Levene test of homoscedasticity.

Differences in the practice of ICM dose calculation among radiologists were evaluated using the ANOVA.

Continuous data were presented as mean and standard deviation while categorical data were presented as counts and percentages. The coefficient of variation (CoV) was calculated as the standard deviation/mean ratio.

Statistical analysis was carried out using SPSS Statistics (SPSS v.24, IBM Inc., Armonk, NY, USA). A P value < 0.050 was regarded as statistically significant.

Results LBW retrospective study

Distributions

A total of 219 patients were screened, 18 of which were excluded for having chronic liver disease (n=13), implanted device (n=4), or congestive heart failure (n=1). Thus, 201 patients were analysed, 106 males (53%) and 95 females (47%), with a mean age of 66±13 years (CoV 20%), mean TBW 72±15 kg (CoV 21%), mean LBW 53±11 kg (CoV 20%), and mean LBW/TBW 74±8% (CoV 11%). The mean BMI was 26 ± 5 kg/m^2 with 9 patients (4%) classified as underweight, 82 (41%) as normal weight, 76 (38%) as overweight and 34 (17%) as obese. Demographics and other data of the study population are presented in **Table 1**.

Table 1. Demographic characteristics of 201 patients of the study population

Item	**Value**
Total no. of patients	201
Gender	106 males (53%)
Mean age (years)	66±13
Mean height (m)	1.66±0.10
Mean TBW (kg)	72±15
Mean LBW (kg)	53±11
Mean percent LBW/TBW (%)	74±8
Mean BMI (kg/m^2):	26±5
Underweight ($BMI<18.5\ kg/m^2$)	*9 (4%)*
Normal weight ($18.5\leq BMI<25\ kg/m^2$)	*82 (41%)*
Overweight ($25\leq BMI<30\ kg/m^2$)	*76 (38%)*
Obese ($BMI\geq 30\ kg/m^2$)	*34 (17%)*

TBW=total bodyweight; LBW=lean bodyweight; BMI=body mass index.
From Zanardo et al. Eur Radiol Exp. 2018

The mean injected amount of ICM was 32 ± 5 gI (CoV 16%). Expressed in terms of gI/kg of TBW or LBW, the mean ICM dose was 0.46 ± 0.06 (CoV 13%) or 0.63 ± 0.09 (CoV 14%), respectively. The mean CT value of the liver was 53 ± 8 HU before ICM injection and 96 ± 13 HU in the portal venous phase, for a mean LCE of 43 ± 9 HU (CoV 21%). These and other data are reported in **Table 2**.

Table 2. Mean iodinated contrast medium dose administered in 201 patients of the study population

Item	Value*	CoV
Amount of injected ICM (g)	32±5 g	16%
Dose of ICM per TBW (gI/kg)	0.46±0.06	13%
Dose of ICM per TBW (gI/kg) according to BMI†:		
Underweight (BMI<18.5 kg/m^2)	*0.56±0.08*	*14%*
Normal weight (18.5≤BMI<25 kg/m^2)	*0.48±0.05*	*10%*
Overweight (25≤BMI<30 kg/m^2)	*0.44±0.04*	*9%*
Obese (BMI ≥30 kg/m^2)	*0.41±0.04*	*10%*
Dose of ICM per LBW (gI/kg)	0.63±0.09	14%
Dose of ICM per LBW (gI/kg) according to BMI ‡:		
Underweight (BMI<18.5 kg/m^2)	*0.68±0.11*	16%
Normal weight (18.5≤BMI<25 kg/m^2)	*0.62±0.08*	13%
Overweight (25≤BMI<30 kg/m^2)	*0.62±0.08*	13%
Obese (BMI ≥30 kg/m^2)	*0.65±0.11*	17%
Liver contrast enhancement (HU) §	43±9	21%
Liver contrast enhancement (HU) according to BMI ‖:		
Underweight (BMI<18.5 kg/m^2)	51±18	35%
Normal weight (18.5≤BMI<25 kg/m^2)	44±8	18%
Overweight (25≤BMI<30 kg/m^2)	42±9	18%
Obese (BMI ≥30 kg/m^2)	40±6	15%

*Data represent mean±standard deviation.
†This trend showed a significant negative association ($P < 0.001$).
‡The comparison was not statistically significant ($P \geq 0.065$).
§Calculated as the difference between the CT value measured in the venous phase and that measured before contrast medium injection.
‖This trend showed a significant negative association ($P = 0.004$).

ICM= iodinated contrast medium; TBW=total bodyweight; LBW=lean bodyweight; BMI=body mass index; gI=grams of iodine; HU=Hounsfield units. *From Zanardo et al. Eur Radiol Exp. 2018*

Correlation analysis

A significant high negative correlation was observed between ICM dose and TBW (r = -0.683; P < 0.001). In particular, the mean ICM dose was 0.56 ± 0.08 gI/kg for underweight, 0.48 ± 0.05 gI/kg for normal weight patients, 0.44 ± 0.04 gI/kg for overweight patients, and 0.41 ± 0.05 gI/kg for obese patients (P < 0.001) (**Figure 1**).

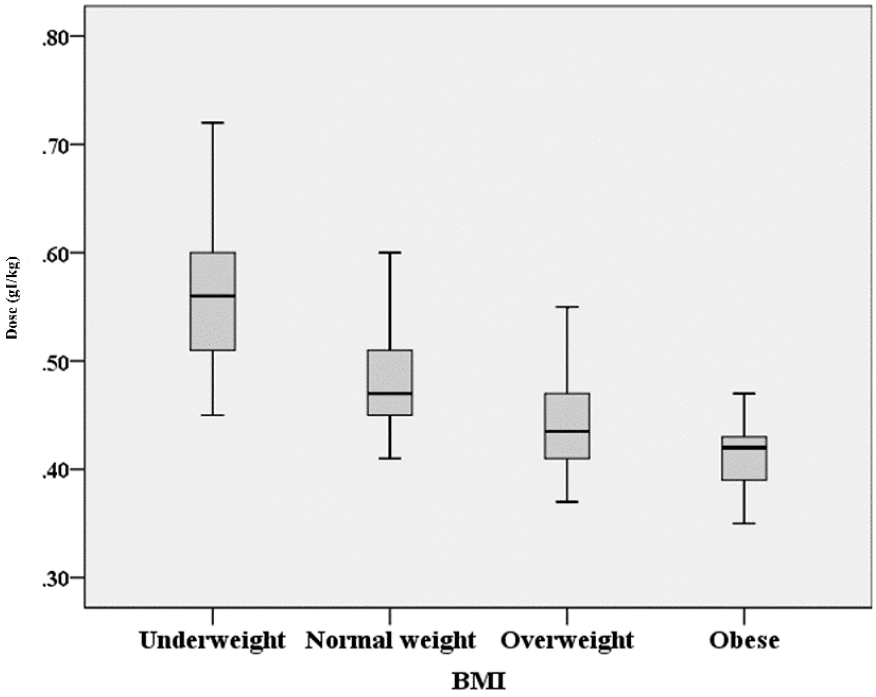

Figure 1: Box plot showing the median dose (in grams of iodine per kg od body weight) per each of the 4 subgroups of the body mass index (BMI) according the WHO (center line). From Zanardo et al. Eur Radiol Exp. 2018

A significant low negative correlation was found between LCE and TBW (r = -0.292; P < 0.001) or LBW (r = -0.316; P < 0.001). A significant low positive correlation was found between LCE and ICM dose in gI/kg of TBW (r = 0.371, P < 0.001) or in gI/kg of LBW (r = 0.333, P < 0.001).

A significant low negative correlation was found between LCE and BMI (r = -0.206; P = 0.003). According to the four subgroups of BMI, the mean LCE was 51 ± 18 HU (CoV 35%) in underweight

patients, 44 ± 8 HU (CoV 18%) in normal weight patients, 42 ± 9 HU (CoV 18%) in overweight patients, and 40 ± 6 HU (CoV 15%) in obese patients with a statistically significant difference of both the mean ($p = 0.004$) and variance ($P < 0.001$).

The mean ICM dose in gI/kg of TBW did not differ significantly among the 8 radiologists, varying from 0.43 to 0.47 gI/kg ($P = 0.510$).

Discussion LBW retrospective study

In this study, we retrospectively evaluated 201 patients undergoing an abdominal CT at our institution. The main finding was the evidence of a kind of "compensation effect", subjectively operated by the radiologists, on the injected ICM dose, always considering its calculation in terms of gI/kg. In fact, we observed a deviation from proportionality between the TBW and the injected ICM dose they declared when questioned about how they decide ICM dose. This was clear in particular for obese patients, which received an ICM dose lower than that theoretically based on the TBW. Indeed, a high negative correlation was found between the patient TBW and the administered ICM dose, meaning that the higher the TBW, the lower the ICM dose.

Although there are no recommendations for obese patients (apart from a general limit of 250 mL reported on the drug information sheet), radiologists preferred to apply a kind of precautionary principle by subjectively reducing ICM dose in obese patients. We could speculate that radiologists have somehow weighted the ICM dose according to a plausible LBW, even being not aware of the exact LBW.

Importantly, although the ICM dose was reduced in obese patients, all CT examinations were judged as diagnostic and no patients received a repeat examination. This allows us to hypothesize a margin for dose reduction, especially in underweight patients, which in our study received a dose in gI/kg significantly higher than obese ones. In fact, the other side of the above-mentioned compensation effect is a potential overdosing in underweight patients, partially due to the fear of a non-diagnostic examination if injected strictly according to the TBW.

Another result of this study is a trend toward a lower and lower variability of LCE from underweight to obese patients (Levene test $P < 0.001$). We speculate that this evidence indirectly demonstrates a better role for LBW to dose ICM rather than TBW. In fact, poor but non-negligible ICM perfusion in the adipose tissue would only increase variability of LCE.

Interestingly, the practice to adjust the ICM dose, unconsciously weighting for the LBW, was observed in all the staff radiologists, without significant differences among them. Of note, this shared

practice spontaneously evolved in the department real-life. In addition, repeat CT examinations due to insufficient parenchymal contrast enhancement has ever been reported.

We also obtained an equivalent ICM dose, i.e. the ICM dose based on the LBW that would have provided the same amount of iodine that was actually administered. In the study population, a mean of 32 ± 5 gI was injected, corresponding to 0.46 ± 0.06 gI/kg of TBW or 0.63 ± 0.09 gI/kg of LBW. Although the latter data was back calculated from the raw data, it is reasonably to think that if 0.63 gI/kg of LBW had been used instead of 0.46 gI/kg of TBW, it would have resulted in an equivalent mean LCE.

The use of LBW instead of TBW on a patient-by-patient base could impact on the overall ICM dose to the population, permitting a more personalized approach to ICM administration and a possible reduction of the total amount of ICM administered to the population. Moreover, as obesity increases the risk for kidney disease (41), a reduction of the overall dose to obese patients represents a further advantage in terms of risk of nephrotoxic effects from iodinated ICM. The associated cost reduction, dependent on changes in administered volume, is another advantage potentially deriving from this approach (10). However, although Awai et al. (38) have already identified LBW as the best indicator for determining the proper amount of ICM, its use has never entered the clinical practice.

When optimising ICM dose, several factors should be taken into account (2). From pharmacokinetics, it is known that drug distribution in the arterial phase mainly depends from the heart function, while in portal venous phase vasoconstriction-vasodilatation play the main role in determining ICM distribution (21,42). We based our results on LCE but a wide variety of para-physiological conditions can affect liver parenchyma in the general population (e.g. steatotic hepatitis, diffuse cirrhosis, previous liver diseases) that can affect LCE.

This study has limitations, first of all its retrospective design and relatively small number of patients, which implied an uneven distribution of patient weights. In addition, we estimated the patient LBW using the James or Boer formulas. Indeed, LBW determined with the aid of a total body composition analyser may yield a more accurate analysis. There are several prediction formulas for

LBW (39,40,43,44) that may yield different results. However, for the aim of our study, the formulas we used are considered the simplest methods for retrospective calculation of the LBW, confirmed by Caruso et al (33).

In conclusion, the ICM dose injected at our institution for abdominal multiphasic CT was highly variable, with obese patients receiving a much lower dose than underweight patients, as a radiologist-driven “compensation effect”. Diagnostic abdominal CT may be obtained using 0.63 gI/kg of LBW and margins for dose reduction do exist.

2. Using Lean Body Weight (LBW) instead of Total Body Weight (TBW) to dose iodinated contrast medium in abdominal CT: a randomized controlled trial

Materials and methods LBW randomized controlled trial

Ethical approval

Our RCT was reported according the CONSORT statement (45). This RCT was approved by the local Ethics Committee (IRCCS Ospedale San Raffaele, Milan, authorization number 160/int/2017), and was performed in a university hospital that is partially supported by Italian Minister of Health. All participants signed a written informed consent form. The trial was registered on clinicaltrials.gov as NCT03384979.

Study design

This was a single center, comparative, double-blinded, two-arm RCT (1:1) comparing LBW-based dosage (experimental group) versus TBW-based dosage (control group) for intravenous administration of ICM in contrast-enhanced abdominal CT. Patient enrolment started in October 2017.

Primary and secondary endpoints

The primary endpoint was the CE of the liver. The secondary endpoints were the CT value of the descending aorta, vena cava, vena porta, and spleen; only for the descending aorta we also calculated the CE.

Inclusion and exclusion criteria

An independent operator prospectively enrolled patients aged ≥ 18 years referred to our Institution for a multi-phase, contrast-enhanced abdominal CT as part of their standard clinical care. Clinical

indication to CT was not fixed and none of the patients underwent the CT for the sole purpose of the study.

Exclusion criteria were: patients needing a CT protocol different from our standard protocol for any reason (e.g. tube voltage different from 120 kVp); history of chronic liver disease (cirrhosis, local or diffuse liver fatty infiltration, or glycogen storage disease); congestive heart failure; prior cardiac valve replacement; restrictive or constrictive pericarditis; implanted devices (pacemakers, defibrillators, insulin pumps); liver steatosis defined as pre-contrast CT values lower than 30 HU; inability to give informed consent.

Randomization and ICM dosages

Patients were randomly assigned to either the TBW or the LBW group using a random generator performed by an operator external to the clinical team. Specifically, the two study groups were:

- TBW group, receiving 0.44 g iodine/kg of TBW;
- LBW group, receiving 0.61 g iodine/kg of LBW.

These two dosages were obtained on the basis of the data reported by us in a retrospective study on 201 patients. Briefly, the former was the mean ICM dose used in our Institution, while the latter was the equivalent dose in terms of LBW that allowed to reach the same liver CE as that obtained using TBW dosage.

Neither the patient or the referral radiologist was aware of which group patients were assigned to.

LBW estimation

The TBW, height, waist circumference, and body mass index (BMI) were obtained. LBW was measured through a balance for bioelectrical impedance analysis (Tanita® mod. SC-240MA, Tokyo, Japan), which allows simultaneously TBW and LBW measurements. Following the BMI international classification of the World Health Organization (37), patients were considered

underweight when BMI was lower than 18.5 kg/m^2, normal weight when BMI was from 18.5 kg/m^2 to 25 kg/m^2, overweight when BMI was from 25 kg/m^2 to 30 kg/m^2, and obese when BMI was higher than 30 kg/m^2.

CT protocol

All patients underwent a contrast-enhanced multi-phase CT scan of the abdomen. All patients were scanned using a 64-row CT unit (Somatom Definition, Siemens Healthineers, Erlangen, Germany) with 120 kVp, tube load from 100 to 200 mAs depending on automatic exposure control system (CARE Dose 4D, Siemens Healthineers, Erlangen, Germany), rotation time 0.5 s, pitch 1, B30f medium smooth kernel reconstruction technique.

Iopamidol (Iopamiro 370; 370 mgI/mL; Bracco Imaging, Milan, Italy) was administered at a dose according to each study group. The ICM was administered intravenously through a 20-gauge needle using an automatic power injector (EmpowerCTA® Contrast Injection System, Bracco Imaging, Milan, Italy) at the rate of 3 mL/s, followed by 50 mL of saline solution at the same rate.

Scan delay was determined using an automated triggering hardware and a dedicated software (Bolus Tracking, Siemens Healthineers, Erlangen, Germany). Specifically, low-dose single-slice images were used to monitor the arrival of ICM into the descending thoracic aorta. When it enhanced over 100 HU, diagnostic scans of the abdomen were acquired after an additional average delay of 18 s for the arterial phase, 48 s for the portal venous phase, and, only in selected cases, 108 s for the nephrogenic phase. For the aim of this study, we analyzed only the portal venous phase.

Image analysis

All images were reviewed independently by a radiology resident (F.M.D.) with four years of experience of abdominal CT, and by a PhD student (M.Z.) with three years of experience in image analysis. For the primary endpoint, CT attenuation measurements were obtained by manually placing a 130-170 mm^2 region of interest in the anterior (III or IVb Couinaud) and in the posterior

(VI Couinaud) segments on a slice containing the main portal vein (**Figure 2**); these two values were averaged. Two different regions of interest were chosen to take into account subtle territorial differences in liver enhancement. Focal hepatic lesions, blood vessels, bile ducts, calcifications, as well as artefacts, if present, were carefully avoided. Liver CE was calculated as the difference between the CT value measured in the portal venous phase and that measured before ICM injection. To do this, regions of interest were copy-pasted from one phase to another. Liver CE was adjusted with amount of iodine injected (adjusted liver CE) expressed as HU/gI.

Moreover, measurements were repeated both in the pre-contrast and portal venous phases w also for the aorta at the level of celiac trunk, spleen, and psoas muscles at L3–L5 level; vena cava and vena porta were measured only in the portal venous phase.

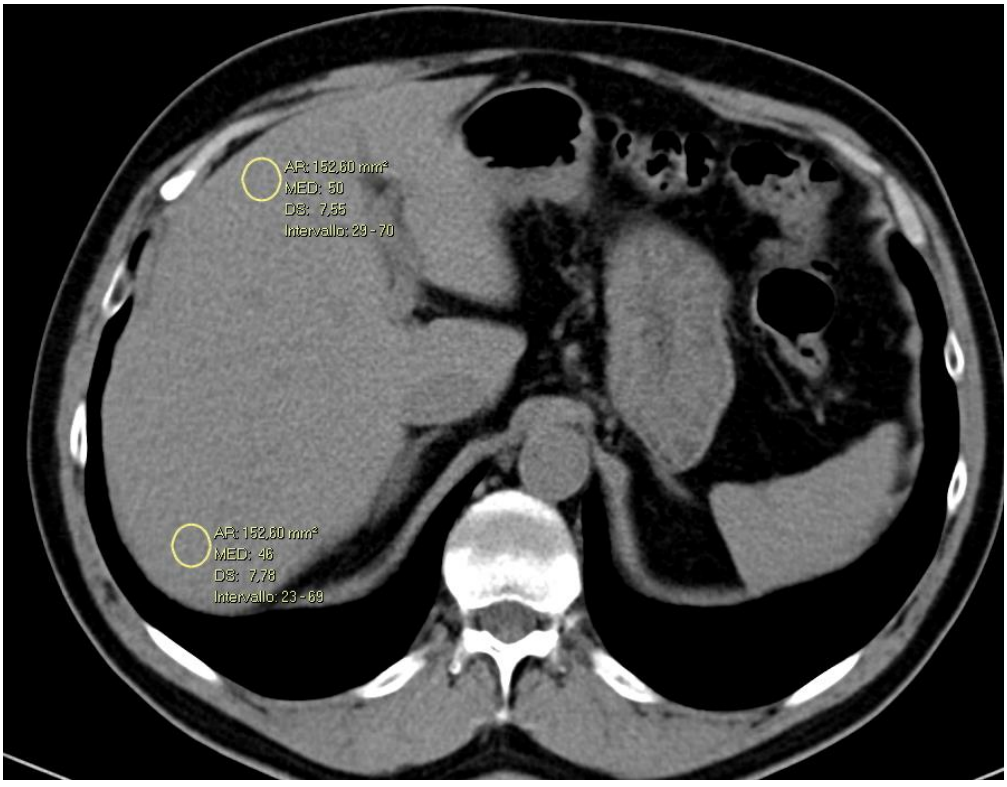

Figure 2: Example of region of interest positioning in the anterior (III or IVb Couinaud) and in the posterior (VI Couinaud) segments in pre-contrast phase in a male patient (65 years old).

Sample size calculation

The sample size was calculated for the primary endpoint, assuming the following: alpha error of 5%, statistical power of 80%, and reduction of the liver CE standard deviation from 7 HU in the TBW group to 5.5 HU in the LBW group [these data were derived from our retrospective study (46)]. A total of 274 patients (137 per group) were needed to detect such a difference using a one-sided F test.

Statistical analysis

Continuous data were presented as mean and standard deviation or median and interquartile interval (IQI) depending on data normality, while categorical data were presented as counts and percentages. Shapiro-Wilks test was used to assess normality of distributions.

For each group, the distribution of liver CE was calculated for the whole population and for the four subgroups of BMI. Between-groups comparisons were performed using the one-way ANOVA or Kruskal-Wallis, depending on the distributions. In particular, the homogeneity of variance or rank spread (the non-parametric equivalent of the variance) of liver CE was verified using the non-parametric Levene's test. Categorical variables were compared using the □2 test. The anatomical structures other than the liver underwent to exploratory analysis only.

As a total of 22 statistical tests are carried out for comparing the two groups, the Bonferroni correction was used. Thus, the threshold for significance was set to 0.05/22=0.002. Statistical analysis was carried out using SPSS Statistics (SPSS v.24, IBM Inc., Armonk, NY, USA).

Pearson's or Spearman's correlation coefficient was calculated for adjusted liver CE depending on normality distribution.

Results LBW randomized controlled trial

Flowchart

A total of 335 patients were enrolled from October, 2017 to October, 2018. Seventeen patients were excluded from randomization due to screening failure: 10 as they declared known liver diseases only after the informed consent signature, while 7 did not perform the CT (n = 3) or performed only an unenhanced CT (n = 4) as per later decision of the radiologist. Thus, 318 patients were randomized and allocated to either the LBW group (n = 157) or the TBW group (n = 161). Thereafter, 8 patients randomized to the LBW group and 9 randomized to the TBW group were drop out as the intended ICM dose was considered too low (n = 10) or too high (n = 7) by the radiologist. Thirty patients (16 patients from the LBW group and 14 from the TBW group) were excluded from analysis due to unknown diffuse liver disease (steatosis, n = 24; cirrhosis, n = 6) discovered only at CT. Thus, statistical analysis was performed on a total of 274 patients, 133 of the LBW group and 141 of the TBW group (**Figure 3**). All distributions were non normal at the Shapiro-Wilk test ($P < 0.014$). Thus, non-parametric statistics were used for all analyses.

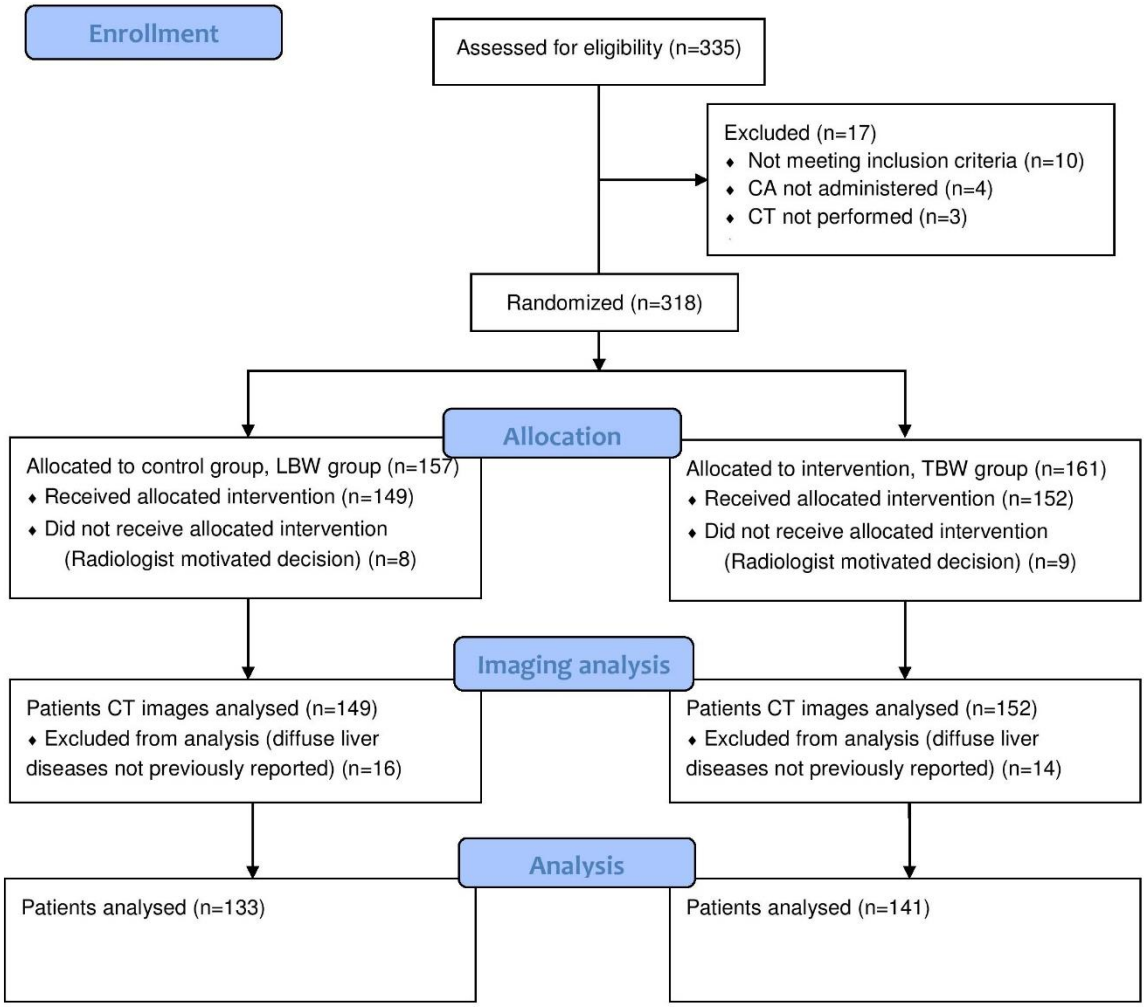

Figure 3: Flow diagram of the progress through the phases of two groups (enrolment, allocation, imaging analysis, and data analysis).

Demographics and baseline characteristics

The demographics distributions are reported in **Table 3**. All comparisons were not statistically significant after the Bonferroni correction ($P \geq 0.023$). The median volume of injected ICM in the LBW group (83 mL [69–96]) was also not significantly different ($P = 0.907$) from that injected in the TBW group (82 mL [72–93]). However, the variability (interquartile range) was significantly higher in the LBW group compare to the TBW group (28 HU vs 21 HU, $P = 0.008$).

The distribution of the pre-contrast liver CT value showed a slightly unbalanced variability between the two groups. Although the medians were 56 HU in both groups, the interquartile range

in the LBW group was higher than that in the TBW group (10 vs 7 HU), although not statistically significant after Bonferroni correction.

Table 3: Patient demographics

	TBW group (n=141)	**LBW group (n=133)**	***P*-value for medians***	***P*-value for variances/rank spread[$]**
Age (years)	70 (61–77)	66 (56–75)	0.023	1.000
Number of males	80 (57%)	73 (55%)	0.758	-
TBW (kg)	68 (60–77)	69 (60–77)	0.999	0.985
Height (cm)	165 (160–174)	165 (160–175)	0.893	0.928
LBW (kg)	50 (42–58)	50 (42–58)	0.995	0.284
BMI (kg/m^2)	24 (22–28)	25 (22–27)	0.777	0.393

*All comparisons performed using the *Mann-Whitney U* test, except for sex (χ^2 test). [$] Non-parametric Levene's test.
TBW = total body weight; LBW = lean body weight; BMI = body mass index.

Primary and secondary endpoints

The median liver CE was 40 (35–46) HU in the LBW group and 40 (35–44) HU in the TBW group, with the comparison being not significant for both the median (P = 0.411) and the rank spread (P = 0.230).

Medians and IQI of CT value and CE in the liver, aorta, and spleen for each contrast phase are summarized in **Table 4**. After Bonferroni correction, there was no significant difference between the two groups for both medians ($P \geq 0.289$) and rank spread ($P \geq 0.013$).

Table 4: Distribution of CT value and contrast-enhancement measured in the anatomical structures analyzed in the study

Anatomical structure	**TBW group (n=141)**	**LBW group (n=133)**	***P*-value for medians***	***P*-value for variances/rank spread[$]**
Liver PC (HU)	56 (53–60)	56 (51–61)	0.905	0.015
Liver AP (HU)	74 (67–81)	73 (65–80)	0.459	0.397
Liver VP (HU)	97 (91–102)	97 (90–105)	0.430	0.013
Liver CE (HU)	*40 (35–44)*	*40 (35–46)*	*0.411*	*0.230*
Aorta PC (HU)	43 (40–45)	43 (40–45)	0.466	0.722
Aorta AP (HU)	267 (237–305)	273 (238–304)	0.764	0.815
Aorta VP (HU)	125 (116–136)	125 (117–134)	0.946	0.463
Aorta CE (HU)	*83 (73–92)*	*83 (74–91)*	*0.767*	*0.699*
Cava VP (HU)	101 (95–110)	104 (95–110)	0.289	0.930
Porta VP (HU)	128 (118–136)	127 (118–139)	0.874	0.234
Spleen VP (HU)	92 (87–98)	94 (87–99)	0.592	0.634

* Mann-Whitney *U* test; [$] Non-parametric Levene's test.
HU = Hounsfield unit; PC = Pre-contrast; AP = Arterial phase; VP = Venous phase; CE =contrast enhancement.

Considering ALCE (ΔHU/g iodine), an inverse strong correlation between ALCE and TBW was found in the TBW group ($r = -0.712$, $P < 0.001$) with linear regression analysis (**Figure 4**), while an inverse moderate correlation between ALCE and LBW was found in the LBW group ($r = -0.546$, $P < 0.001$) (**Figure 5**).

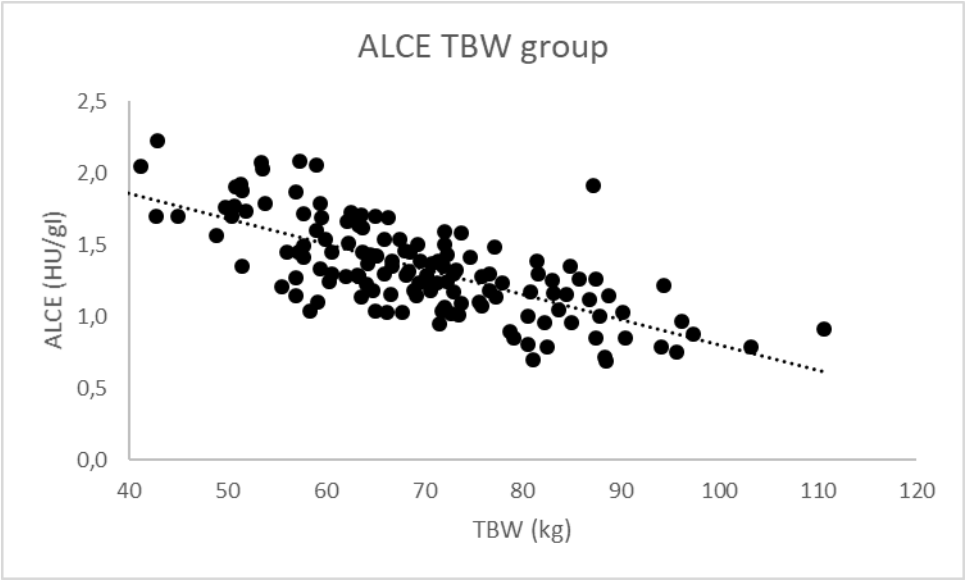

Figure 4: Scatter plot showing the relationship between ΔHU/g iodine of the liver in the portal venous phase and TBW of the TBW group. Inverse strong correlation exists in the TBW group (r = -0.712, P *< 0.001) with a linear regression analysis. Regression line is represented with dotted fitting line.*

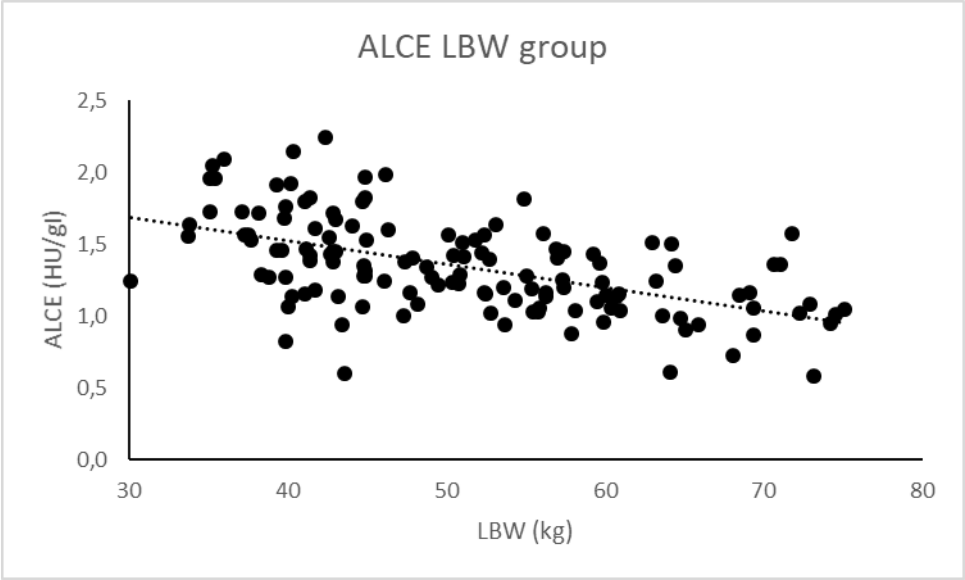

Figure 5: Scattergram showing the relationship between ΔHU/g iodine of the liver in the portal venous phase and LBW of the LBW group. Inverse moderate correlation exists in the LBW group (r = -0.546, P *< 0.001) with a linear regression analysis. Regression line is represented with dotted fitting line.*

Suboptimal LCE (<40 HU) was found in 64/133 (48%) patients in the LBW group and 69/141 (49%) in the TBW group, with no statistically significant difference (P = 0.893). No repeated examination was requested for any patient.

At subgroup analysis, considering BMI categories, no statistically significant differences were found in terms of LCE (P > 0.207), as shown in **Table 5** and **Figure 6**.

Table 5: Medians and interquartile intervals of LCE values for subgroups: BMI classes and sex.

	TBW group (n. patients)	LBW group (n. patients)	Test *U Mann-Whitney*
All patients	40 (35–44) (141)	40 (35–46) (133)	P = 0.411
BMI <18.5 kg/m²	36 (34–39) (6)	37 (34–39) (5)	P = 0.999
BMI 18.5-25 kg/m²	40 (35–44) (71)	41 (36–47) (67)	P = 0.207
BMI 25-30 kg/m²	40 (36–44) (47)	39 (36–46) (51)	P = 0.921
BMI >30 kg/m²	39 (35–48) (17)	39 (35–43) (10)	P = 0.570
Males	40 (35–44) (80)	43 (38–48) (73)	P = 0.003
Females	40 (35–46) (61)	37 (34–42) (60)	P = 0.034

TBW = total body weight; LBW = lean body weight; BMI = Body mass index

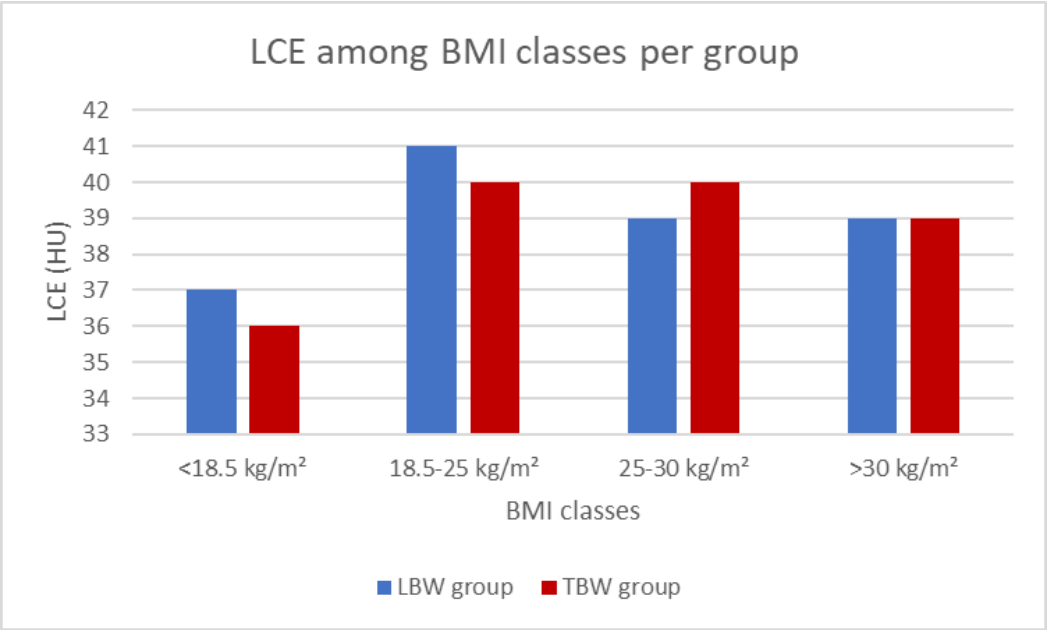

Figure 6: Bar chart representing median LCE values among BMI classes. No statistically significant differences were found: BMI <18.5 kg/m²: P = 0.999, BMI 18.5-25 kg/m²: P = 0.207, BMI 25-30 kg/m²: P = 0.921, BMI >30 kg/m²: P = 0.570.

At subgroup analysis, a significant difference was found between LCE in males: 43 (38–48) HU for LBW group and 40 (35–44) HU for the TBW group (P = 0.003), and in females: 37 (34–42) HU for LBW group and 40 (35–46) HU for TBW group (P = 0.034), as reported in **Table 5**.

Discussion LBW randomized controlled trial

This randomized controlled trial showed that dosing ICM using LBW in a general population (no athletes) does not reduce LCE variability compared to a TBW-based approach, thus, the initial hypothesis was rejected. Considering a negative result as a finding that does not show impact or change (47), clinical studies with negative results may not be published as frequently as significant studies (48), leading to a publication bias in scientific research (47,49–51). We may assume that if we do not publish negative (or nonsignificant) results, then the knowledge that something is ineffective (or less effective) will be not communicated to the scientific community. We believe that negative data deserve to be published, as long as they highlight a lack of knowledge in a specific topic or refute an evidence in order to reach a comprehensive view of a problem or its solution (47).

The statistically significant difference between TBW and LBW groups in terms of age is probably due to a chance and this difference should not have impact on our results. As expected, no difference was found in terms of mean of LCE: we retrospectively calculated the equivalent dose for LBW group to reach at least the same LCE of the TBW group (46), while a significant difference was found for variances.

Ho et al. (22) and Kondo et al. (25,26) reported that calculation of ICM dose on the basis of patient LBW led to increased patient-to-patient uniformity of hepatic parenchymal and vascular enhancement (52). The results in the study published by Kondo et al. in 2013 (30) differ from our findings. We did not find a significantly different patient-to-patient variability in terms of LCE when dosing ICM using LBW instead of TBW. This is probably due to two main causes. First, we used a relatively lower dose (0.61 vs 0.71 g iodine/kg of LBW) that could have reduced the effect of LCE optimisation. This was a back-calculated equivalent dose based on our experience (46). Of note, no supplemental ICM injection was needed due to any enhancement judged to be clinically insufficient. Second, our patients are coming from Western populations, with a higher average TBW (69 ± 13 kg, mean ± standard deviation) compared to the Asian populations studied by Kondo et al. (55 ± 10 kg) (30).

Regarding LCE found in both groups, almost 50% of all patients was under the suboptimal level (< 40 HU) suggest by Heiken et al. in 1995 (7), but all examinations were considered diagnostic by our team. In the last decade, the capability of detection, as well as the technical components of the CT hardware and software improved a lot. So, the "sufficient" LCE should be updated and reconsidered in the light of new technologies and new reconstruction algorithms that allow a ICM dose reduction. Indeed, as recently demonstrated by Bellesi et al. (53), iterative reconstruction-based methods provided a 60% noise reduction and a 70% dose reduction, preserving image quality and low-contrast detectability for human radiological evaluation. Moreover, full model-based iterative reconstruction (MBIR) can reduce image noise by 58.6% and increased SNR and CNR by 143.6% and 165.7%, respectively and using a protocol with 19.3% reduced ICM dose (54). This confirming that full MBIR are more effective than others adaptive statistical iterative reconstruction algorithms: contrast-to-noise ratio and spatial resolution of full MBIR are significantly higher, and full MBIR at low dose levels led to better low-contrast detectability (55).

With the aforementioned technical improvements, new optimal ICM dosages should be adopted, as described by Goshima et al. for the detection of liver metastasis at 80-kVp CT (56). In another recent article, Mertens et al. (57) found that body weight-adapted ICM injection protocols result in more homogeneous enhancement of the liver parenchyma at 90 kVp in comparison to a fixed ICM volume with comparable objective and subjective image quality, whereas overall ICM volume can be safely reduced in more than half of patients. Moreover, in a recent paper published by Walgraeve et al. (58), an adjusted patient-tailored ICM volume based on body surface area (BSA) and heart rate lead to a decrease ICM volumes in women and low to normal BMI patients and to achieve more consistent contrast enhancement across different BMI-groups in venous phase abdominal CT. On the other side, a report described that none of the tested body size parameters among the height, BMI, LBW, TBW or BSA demonstrated any significantly better correlation with hepatic parenchymal or aortic enhancement than did TBW (59).

In this context, another most promising area of health innovation is the application of artificial intelligence in medical imaging (60). We can speculate that in the next few years computational models or algorithms based on patient data could provide a personalised ICM dosage, considering all factors involved (61) in order to obtain the highest contrast enhanced images quality, with the lowest ICM dose.

Our contribution was to show that LBW alone is not sufficient to homogenize the variability of LCE across different patient morpho-physio characteristics and that also gender is a factor involved in determining LCE.

This RCT has limitations. First, it is a monocentric study. Second, we enrolled patients with common morphometric characteristics in our region so that the results are not applicable to different populations. Third, we did not evaluate image quality outside contrast-enhancement nor the diagnostic capability of the technique, being the study focused on the LCE. Moreover, although Hamer et al. (36) defined steatotic hepatitis when liver parenchyma has an average CT values on unenhanced images lower than 40 HU, we excluded patients with CT values below 30 HU in the unenhanced scan. As a consequence, low grade of steatosis has been presumably included in our study population. Moreover, the radiologist who performed the CT could drop patients from the study when they acknowledged that the predetermined amount of ICM was improper for that specific case.

In conclusion, ICM doses based on TBW and LBW lead to a similar LCE with a significantly larger variation for LBW group, thus negating the study hypothesis and highlighting the knowledge gap about factors affecting LCE. Tailoring ICM dose on LBW lead to a higher LCE variability, assuming that others physiological factors are involved in LCE. Radiologists probably need a model of LCE (and in genera body parenchymal organs) taking into consideration at least TBW, LBW, gender, BSA, and cardiac output. A work for the future.

3. Technique, protocols, and adverse reactions for contrast-enhanced spectral mammography (CESM): a systematic review

Introduction CESM systematic review

Between the 1960s and 1970s, randomized controlled trials proved that screen-film mammography is a tool for breast cancer screening that yields to reduced breast cancer mortality (62). Since early 2000s, screen-film mammography was progressively replaced by digital mammography (DM), which improved performance especially in women under 50 and in case of dense breasts, even though providing an intrinsically inferior spatial resolution (63). In the last two decades, digital breast tomosynthesis granted substantial further improvements (64,65), increasing cancer detection rate and reducing the recall rate (66).

Contrast-enhanced mammography is the combination of x-ray mammography with the intravenous administration of ICM (67). It was first attempted using a digital subtraction technique (68–70), but this approach was soon abandoned due to difficulties in co-registration of unenhanced and contrast-enhanced images (71,72). In the last two decades, contrast-enhanced spectral mammography (CESM) has been introduced, based on dual-energy breast exposure (about 26–33 kVp and 44–50 kVp) after contrast administration (71,73). CESM allows for the visualization of enhancing findings over the normal unenhancing breast tissue, exploiting the increased contrast uptake of malignancies (67,71,74).

Original studies have investigated the use of CESM in a number of settings, such as evaluation of symptomatic women (75–78), screening recalls (79,80), local staging (81–90), pre- and post-operative evaluations (81,82,91–94), and neoadjuvant chemotherapy response monitoring (95–98). In 2016, a first meta-analysis on CESM described a high pooled sensitivity (98%) albeit with a relatively low specificity (58%) (99), the latter due to the paucity of studies, partly burdened by inexperience. A more recent meta-analysis (100) reported globally satisfying data for CESM pooled

sensitivity (89%) and specificity (84%), proposing it as an alternative to contrast-enhanced MRI and even suggesting CESM as a "useful triage test for initial breast lesions assessment" (99).

A time delay between the first appearance of new imaging techniques and their implementation in diagnostic routine is expected for many reasons, including not only the definition of indications but also the reproducibility of results. The latter is strongly influenced by technique details, such as – in the field of contrast-enhanced breast imaging – contrast medium concentration, dose and injection rate, breast compression and positioning, exposure parameters, and acquisition protocol. Indeed, the fact that CESM is variably performed across different centres, without an agreed and standardized technique, does not come as a surprise: this circumstance echoes the one observed for contrast-enhanced breast MRI in the 1990s, now settled by the publication of detailed international guidelines (101–104).

Therefore, the aim of this work was to review CESM studies, focusing on adopted technique, contrast medium issues, and acquisition workflow. This effort is crucial for future CESM investigations to be reproducible and comparable.

Materials and methods CESM systematic review

Study Protocol

No ethics committee approval was needed for this systematic review. The study protocol was registered on PROSPERO (https://www.crd.york.ac.uk/prospero/), the international prospective register of systematic reviews (105). This systematic review and meta-analysis was reported according to the Preferred Reporting Items for Systematic reviews and Meta-Analyses (PRISMA) statement (106).

Search Strategy and Eligibility Criteria

In February 2019, a systematic search was performed using MEDLINE (PubMed, www.pubmed.gov), EMBASE (Elsevier) and the Cochrane Library (Cochrane Database of Systematic Reviews, Cochrane Central Register of Controlled Trials for articles that reported or may have reported CESM technique. A controlled vocabulary (medical subject headings in PubMed and EMBASE thesaurus keywords in EMBASE) was used. The search string was: (cesm OR 'contrast enhanced spectral mammography'/exp OR 'dual energy mammography' OR 'contrast enhanced digital mammography'/exp OR 'contrast-enhanced mammography' OR 'dual-energy subtraction mammography' OR cedm OR cedsm OR 'contrast enhanced spectral imaging' OR 'high energy and low energy digital mammography') AND ('procedures'/exp OR 'method' OR 'methods' OR 'procedure' OR 'procedures' OR 'technique' OR 'acquisition'/exp OR 'contrast medium'/exp OR 'contrast agent' OR 'contrast dye' OR 'contrast material' OR 'contrast media' OR 'contrast medium' OR 'radiocontrast medium' OR 'radiography contrast medium' OR 'roentgen contrast medium' OR 'image processing'/exp OR 'image processing' OR 'image processing, computer-assisted' OR 'processing, image').

The search was limited to original studies on humans published in English, French, and Spanish on peer-reviewed journals, with an available abstract. No publication date limits were applied. Screening was performed by two independent readers (A.C. and M.Z., with 1- and 3-year experience

in breast imaging, respectively) based only on title and abstract. Eligible articles were those that reported in the title or in the abstract the use of CESM technique or that could have contained these data in the manuscript. After downloading eligible articles, the full text was read for a complete assessment. Finally, references of included articles were hand-searched to check for further eligible studies.

Data extraction

Data extraction was performed independently by the same two readers who performed the literature search. Disagreements were settled by consensus. For each analysed article, year of publication, institution (such as hospitals, imaging facilities, breast units including radiology sections, or any other type of centre in which CESM is performed) and country origin as well as research groups, design, number of patients, and demographics were retrieved. Mammography unit, vendor, radiation dose and technical features such as low- and high-energy kVp, anode/filter combinations and exposure parameters were also extracted. Moreover, contrast medium type, dose and concentration were retrieved, as well as injection modality, if manual or automated, flow rate and additional post-contrast saline flush or "bolus chaser" if present. Furthermore, mild, moderate or severe adverse reactions to ICMs were extracted alongside strategies for their prevention. Regarding the acquisition protocol, time between contrast injection and first image acquisition and maximum examination duration were extracted. Regarding the order of views, we reported the acquisition sequence of the standard mammographic projections considering the craniocaudal (CC) and the mediolateral oblique (MLO) views, including the first side acquired. Missing data were requested to authors.

Evidence synthesis

To avoid risk of data duplication bias, in case of articles published by the same research group, we considered the possibility of performing subgroup analysis: therefore, before delving into further analysis of protocol description, we chose to change our viewpoint from the number of articles

reporting a specific protocol to the minimum number of times a protocol was reported by a single research group.

Regarding the pooled rate of adverse reactions related to ICM administration across studies, statistical analysis was performed using Comprehensive Meta-Analysis v2.2.057 (Biostat, Englewood, NJ, USA) using the meta-analysis model "Number of events and study population". I^2 statistics was first calculated to assess heterogeneity and the fixed-effect model was used to provide the rate of adverse reactions and 95% of confidence intervals (CI). The risk of publication bias was assessed by visually inspecting funnel plot and performing the Egger test (107).

Results CESM systematic review

Literature search and characteristics of the analysed studies

A flowchart of study selection is shown in **Figure 7**.

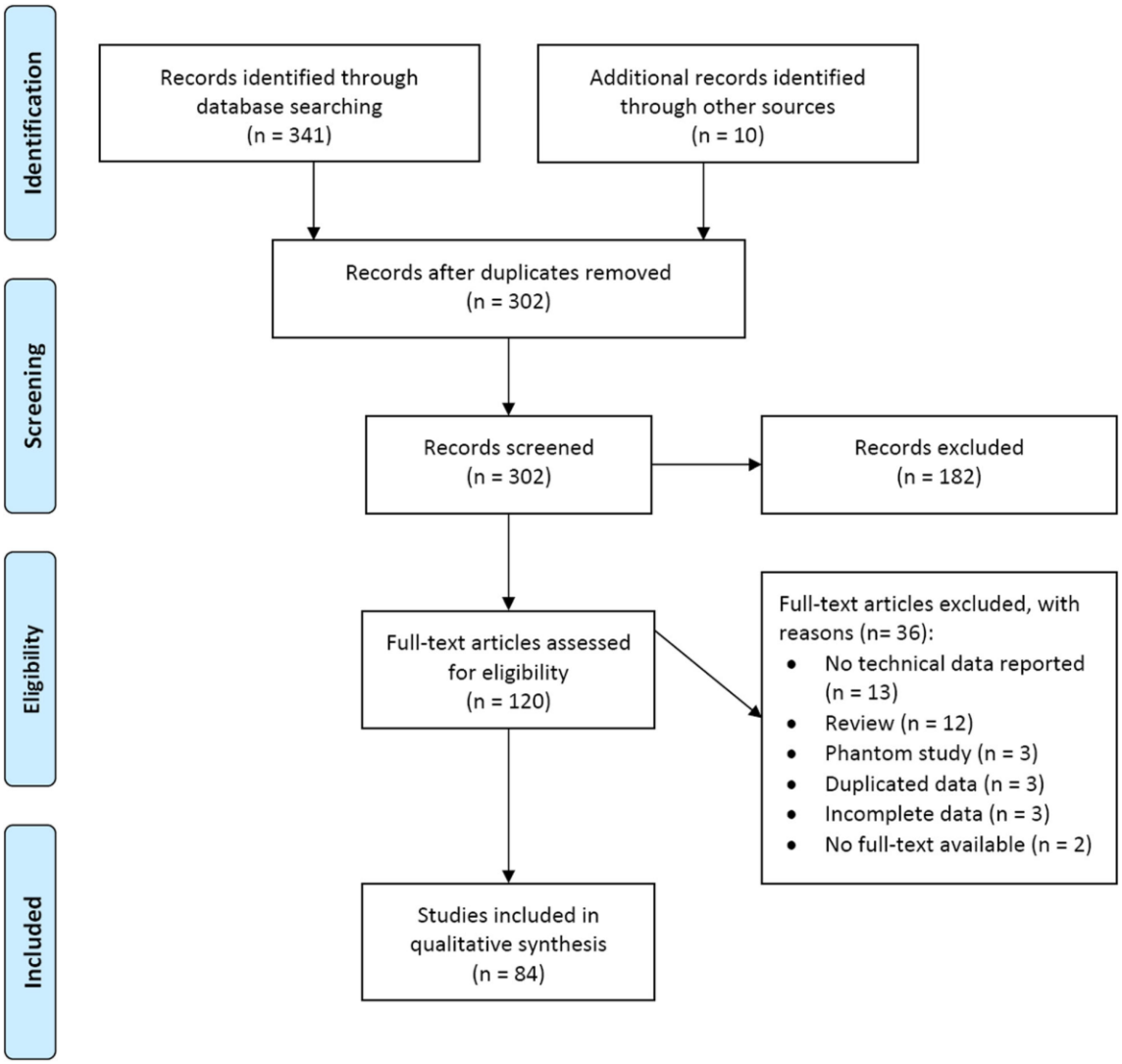

Figure 7: Flowchart of the study selection and exclusion for articles on contrast-enhanced spectral mammography. From Zanardo et al. Insight into Imaging. 2019

Of 120 retrieved articles, 84 (70%), published between 09/2003 and 01/2019, were analysed (68,69,80–89,70,90–98,108,71,109–118,74,119–128,75,129–138,76,139–148,77,149–158,78,159–162,79); 40/84 (48%) being retrospective and 44/84 (52%) prospective (39/44 monocentric, 89%, and 5/44 multicentric, 11%); 54/84 (64%) articles investigated CESM diagnostic performance, whereas

30/84 (36%) focused on technical features. The geographic distribution of research groups is depicted in **Figure 8**.

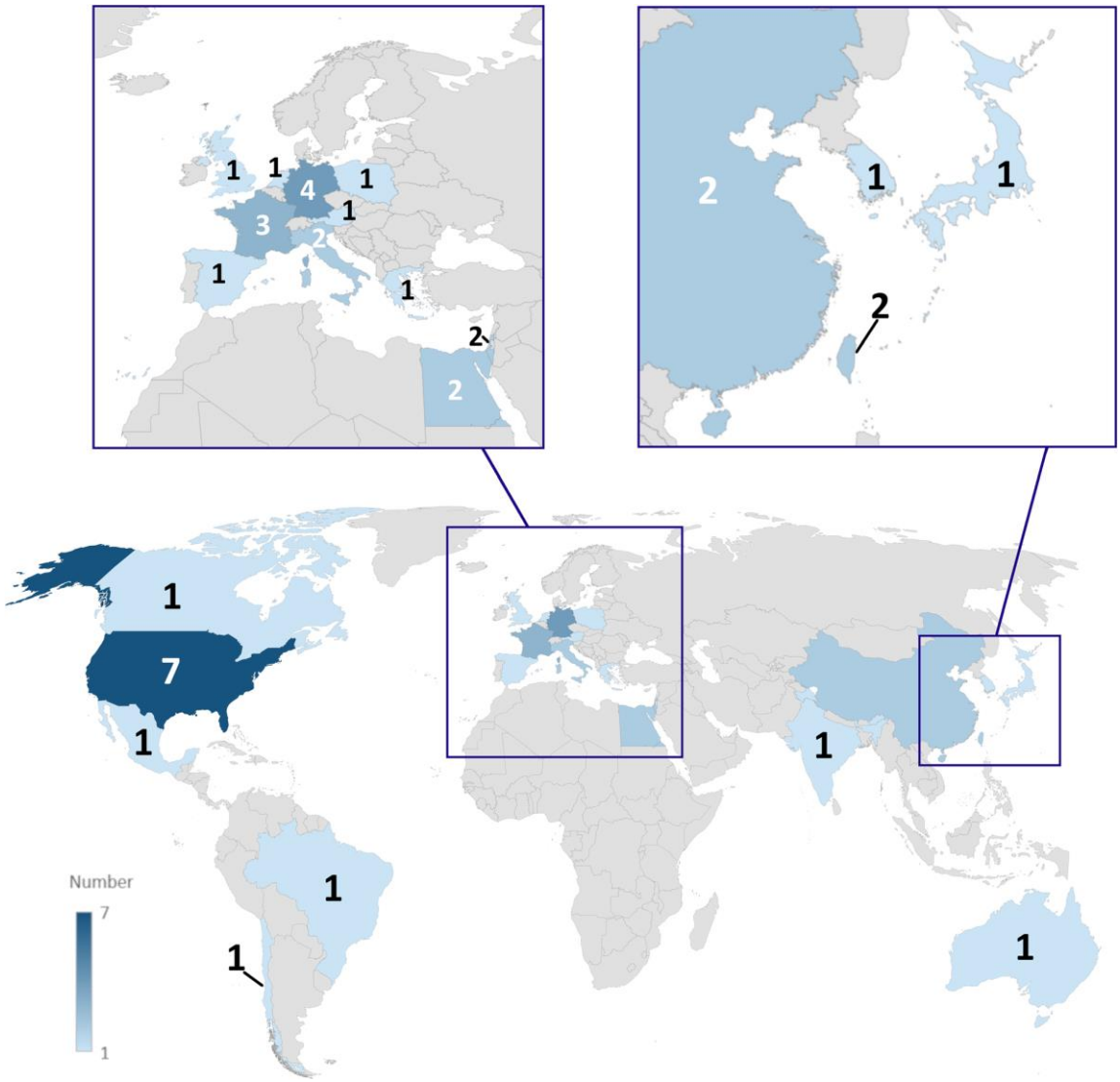

Figure 8: Geographic distribution of research groups which published results of clinical applications of contrast-enhanced spectral mammography. From very light blue to dark blue, the number of groups progressively increases from 1 to 7; grey colour means no publications. From Zanardo et al. Insight into Imaging. 2019

Population setting

Data synthesis is reported in **Table 6**.

Table 6: Main characteristics of the 84 analysed studies.

Author / year	Number of patients	Contrast medium type	Concentration (mgI/mL)	Dose (mL/Kg)	Flow rate (mL/s)	Time before imaging (seconds)	Total exam time
Houben 2019	147	Iopromide	300	1.5	3	120	
Barra 2018	33	Iohexol	300	1.5	3	120	B
Bicchierai 2018	40	Iopromide	370	1.5	3	120	B
Danala 2018	111	Iohexol	350	1.5	3	120	B
Deng 2018	141	Iohexol	350	1.5	3	120	B
Helal 2018	300	Iohexol	300	1.5	3	120	B
Kim 2018	84	Iohexol	350	1.5	2	120	B
Klang 2018	953	Iopamidol	370	1.5	3	120	B
Łuczyńska 2018	82	Iopromide	370	1.5	3	120	B
Moustafa 2018	160	Iohexol	300	1.5	3	120	B
Navarro 2018	465	Ioversol	320	1.5			B
Patel 2018 (01)	65	Iohexol	350	1.5	3	120	A
Patel 2018 (02)	50	Iohexol	350	1.5	3	120	B
Patel 2018 (03)	30	Iohexol	350	1.5	3	120	B
Phillips 2018	45	Iohexol	350	1.5	3	120	
Sorin 2018	611	Iopamidol	370	1.5	3	120	B
Tohamey 2018	178	Iohexol	300	1.5	3	120	B
Travieso-Aja 2018	158			1.5	3	120	B
Xing 2018	235	Iohexol	350	1.5	3	120	B
Barra 2017	11	Iohexol	300	1-2	3	120	B
Bhimani 2017	2303	Iopamidol	370	1.5	2	120	B
Fallenberg 2017	155	Iobitridol	300	1.5	3	120	A
Gluskin 2017	5	Iohexol	350	1.5	3	150-180	A
Helal 2017 (01)	98	Iohexol	300	1.5	3	120	B
Helal 2017 (02)	30	Iohexol	300	1.5		120	
Houben 2017	839	Iopromide	300	1.5	3	120	
Iotti 2017	54	Ioversol	350	1.5		120	
James 2017	173	Iohexol	350	1.5	3	120	A
Jochelson 2017	309	Iohexol	350	1.5	3	150-180	B
Knogler 2017	11	Iomeprol	400	2	3.5	90	
Lee-Felker 2017	52	Iohexol	350		3	120	B
Lewis 2017	208	Iohexol	350	1.5	3	120	B
Li 2017	48	Iopamidol	370	1.5	1.5-2		B
Mori 2017	72	Iohexol	300	1.5	3	120	
Patel 2017 (01)	88	Iohexol	350	1.5	3	120	B
Patel 2017 (02)	410	Iohexol	350	1.5	3	120	B
Phillips 2017	38	Iohexol	350	1.5	3	120	B
Richter 2017	118	Iopromide	300	1.5	2-3	120	
Saraya 2017	34	Iohexol	300	1.5	4		C
Savaridas 2017	66			1.5	3	120	B
Sogani 2017	278	Iohexol	350	1.5	3	150	A
Ali-Mucheru 2016	351	Iohexol	350	1.5	3	120	B
Ambicka 2016	82	Iopromide	370	1.5	3	120	B
Brandan 2016	18	Ioversol	300		4	60	B
Cheung 2016 (01)	256	Iohexol	350	1.5	3	120	A
Cheung 2016 (02)	87	Iohexol	350	1.5	3	120	B
Kamal 2016	239	Iohexol	300	1.5	3	120	B
Kariyappa 2016	44	Iomeprol	350	1.5	3	120	B
Knogler 2016	15	Iomeprol	400	2	3.5	60-90	
Lalji 2016	199	Iopromide	300	1.5	3	120	
Łuczyńska 2016 (01)	116	Iopromide	370	1.5	3	120	B

Łuczyńska 2016 (02)	193	Iopromide	370	1.5	3	120	B
Tardivel 2016	195	Iobitridol	300	1.5	3	120	B
Tennant 2016	99						
Tsigginou 2016	216	Iopromide	300	1.5	2-3	120	B
Wang 2016	68	Iohexol	350	1.5	3	120	A
Yagil 2016	200	Iopamidol	370	1.5	3	120	B
Chou 2015	185	Iohexol	300	1.5	2	120	B
Elsaid 2015	34	Iohexol	300	1.5	3		B
Hobbs 2015	49	Iohexol	350	1.5	3	120	B
Kamal 2015	168	Iohexol	300	1.5	3	120	B
Lobbes 2015	87	Iopromide	300	1.5	3	120	
Łuczyńska 2015 (01)	174	Iopromide	370	1.5	3	120	B
Łuczyńska 2015 (02)	102	Iopromide	370	1.5	3	120	
Badr 2014	75	Iohexol	300	1.5		120	B
Blum 2014	20	Iopamidol	300	1.5	3	120	
Cheung 2014	89	Iohexol	350	1.5	3	120-180	B
Fallenberg 2014 (01)	118	Iobitridol	300	1.5	3	120	B
Fallenberg 2014 (02)	80	Iobitridol	300	1.5	3	120	B
Francescone 2014	88						
Jeukens 2014	47	Iopromide	300	1.5	3	120	
Lobbes 2014	113	Iopromide	300	1.5	3	120	
Łuczyńska 2014	152	Iopromide	370	1.5	3	120	B
Mokhtar 2014	60	Iohexol	300	1.5		120	A
Travieso-Aja 2014	136			1.5	3	120	B
Hill 2013	98	Iobitridol	300	1.5	3	120	B
Jochelson 2013	82	Iohexol	350	1.5	3	150-300	B
Dromain 2012	110	Iobitridol	300	1.5	3	120	A
Diekmann 2011	70	Iopromide	370	1	4	60/120/180	A
Dromain 2011	120	Iobitridol	300	1.5	3	120	A
Dromain 2006	20	Iohexol	300		3	30	B
Diekmann 2005	21	Iopromide	370	1	4	60/120/180	A
Jong 2003	22	Iohexol	300			60	B
Lewin 2003	26	Iohexol	350		4-5	150	

A = total exam time <5 min; B = total exam time between 5 and 10 min; C = total exam time >10 min. *From Zanardo et al. Insight into Imaging. 2019*

The number of patients ranged from 5 (122) to 2,303 (74), for a total of 14,012 patients, with mean or median age ranging from 45 years (98) to 66 years (81). In 29/84 studies (35%), CESM was performed on patients from comprehensive databases of heterogeneous settings, such as pre- or post-operative evaluation, adjuvant or neoadjuvant chemotherapy response monitoring, equivocal cases at conventional imaging, etc. The remaining 55 studies (65%) were individually centred on a unique setting. Twenty-seven studies (32%) performed CESM on suspicious cases from conventional imaging and screening recalls, 11 studies (13%) in a first-line screening setting, 7 (8%) performed

CESM exclusively for known cancer staging, 4 (5%) in a pre-operative setting, 4 (5%) to assess and monitor the response to adjuvant chemotherapy, 2 (2%) in a post-operative setting.

Timing of CESM examination with menstrual cycle was reported only in 18/84 studies (21%). In 10/18 (56%) articles it was mentioned but not applied, in 6/18 (33%) it was applied with a feasibility window between the 5^{th} and 14^{th} day of menstrual cycle; in 2/18 (11%) CESM was synchronously performed with MRI in different phases of menstrual cycle to evaluate and compare background parenchymal enhancement.

Technical features and parameters

In seventy out of 84 studies (83%) different systems from General Electric Healthcare (Chicago, IL, USA) were used, all with a prototype or a commercial release of the SenoBright upgrade which is required to perform dual-energy contrast-enhanced imaging. Twelve out of 84 articles (14%) reported the adoption of Selenia Dimensions mammography unit (Hologic Inc., Marlborough, MA, USA), while the remaining 2/84 (3%) studies were conducted with a Siemens Healthineers (Erlangen, Germany) mammography system (Mammomat or Mammomat Inspiration).

The type of ICM used in CESM examinations was not reported in five articles (76,82,123,125,134), while in the remaining 79 studies (94%, for total 13,465 patients, 96%) six different molecules of were used: Iohexol was the most frequently employed, being used in 42/79 studies (53%) for a total of 5,049/13,465 patients (37%), followed by Iopromide (18/79 studies, 23%, for 2,798/13,465 patients, 21%), while Iobitridol, Iomeprol, Iopamidol, and Ioversol were administered in the remaining studies (19/79 studies, 24%, for 5,618/13,465 patients, 42%). Iohexol was utilized at a concentration of 350 mg iodine/mL (25/42 studies, 60%, for 3,330/5,049 patients, 66%) or 300 mg iodine/mL (17/42 studies, 40%, for 1,719/5,049 patients, 34%). Iopromide was also administered at two different concentrations: 370 mg iodine/mL (10/18 studies, 56%, for 1,032/2,798 patients, 37%) and 300 mg iodine/mL (8/18 studies, 44%, for 1,766/2,798 patients, 63%).

Of the 69 studies including a specification of the contrast injection modality, 59 (85%) utilized an automated power injector (10,584/11,725 patients, 90%) while manual contrast injection was carried out in the remaining 10 (15%) (68,70,78,83,86,109,115,132,155,159) for a total 1,141/11,725 patients, 10%.

ICM dose, detailed in 77 studies, was fixed at 1.5 mL/kg in 72 (93%) of them for a total of 13,559/13,687 (99%) patients. ICM flow rate, reported in 76/84 studies (90%), was most frequently fixed at 3 mL/s (65/76 studies, 86%); the 11 remaining articles detailed a flow rate ranging from 2 to 5 mL/s. Thirty-five out of 84 (42%) articles for a total 8,734/14,012 patients (62%) also mentioned the use of additional post-contrast saline flush or "bolus chaser", 19 of them (54%, for a total 4,477/8,734 patients, 51%) likewise detailing a saline amount ranging from 10 to 30 mL.

Of 69 studies detailing the kVp of both low- and high-energy acquisitions, all but one (99%) acquired low-energy images between 26 and 33.2 kVp, which is the peak kilovoltage threshold of iodine, while all 69 acquired high-energy images well above this threshold, i.e. between 44 and 50 kVp. The anode/filter combination was reported by 42/84 studies and is highly characteristic of the given manufacturer. Exposure parameters were unambiguously reported only in one study, whereas in 5 early studies they were manually adjusted according to breast thickness and density; other 35 studies declared an automatic regulation of these parameters performed by the mammography unit.

Regarding the radiation dose, data were scarcer: even though 45/84 articles (54%) mentioned this aspect, 17/45 (31%) did it without exhibiting original information but reporting observations from previous studies, therefore restricting the number of studies with new data to 28/84 (33%). Of these 28 studies, 19 (68%) provided an average glandular dose (AGD) value, 3 (16%) of them calculating it per-patient ranging 1.5–6.9 mGy (69,70,116), 5/19 (26%) per-breast ranging 2.19–7.15 mGy, and the remaining 11 (58%) reporting a per-view AGD ranging from 0.43 (119) to 2.65 mGy (161). A comparison with DM was mentioned in 17 studies: only 1 (6%) documented a dose reduction (-2%) for CESM compared to DM (90), while other 16 (94%) reported an increase in AGD ranging between 6.2% (145) and 100% (136). However, it is worthwhile to notice that 3 studies specifically

contrived to assess CESM radiation doses reporting an AGD increase of 42% (114), 78% (142), and 80% (118).

Acquisition protocols

Studies reporting the interval between contrast injection and the first image acquisition were 78 out of 84 (93%), for a total 13,244/14,012 patients (95%) and 65 (83%) of them (12,278/13,244 patients, 93%) had it fixed at 120 seconds.

Sixty-six out of 84 articles (79%, for a total 11,900/14,012 patients, 85%) gave an indication of the acquisition time after contrast injection: in 12/66 (18%, for total 1,381/11,900 patients, 11.6%) the exam was completed in less than 5 minutes, in 52/66 (80%, for total of 10,485/11,900 patients, 88.1%) between 5 and 10 minutes, while in 1/66 (2%, for total 34/11,900 patients, 0.3%) the duration exceeded 10 minutes.

The outline of the image acquisition sequence remains more variable. Ten out of 84 studies (12%), accounting for 2,734 patients (19%) did not clearly describe it and did not provide a reference to other protocols, while 3/84 (4%, for total 103/14,012 patients, 1%) employed a curtailed and side-insensitive acquisition sequence. Adherence to standard but unspecified digital mammography protocols was declared by 29/84 (34%) studies, for total 3,741/14,012 patients (27%). The other half of the articles analysed (42/84, accounting for 7,434/14,012 patients, 53%) unequivocally detailed an acquisition sequence. Of these 42 studies, 14 (34%, for total 2.048/7.434 patients, 28%) adopted a projection order that was conventionally agreed upon, while the other 28 (66%, accounting for 5,386/7,434 patients, 72%) based their acquisition sequence on the presence of previous suspect or clearly pathologic findings.

Eighty-four articles came from 36 different research groups. Subgroup analysis according to research groups showed that 17 acquisition sequences based on a conventionally agreed projection order were executed in 15 research groups. As described in **Figure 9**, the most common sequence description, reported by 6/17 (35%) institutions, was MLO - MLO - CC - CC (in order of acquisition),

without any further indication about the first side to be examined (right or left or side with/without suspicious lesion or already diagnosed cancer). The second most common sequence (4/17, 24%) was CC - CC - MLO - MLO with the first projection standardized on the right side (independently of pathology or with suspected pathology).

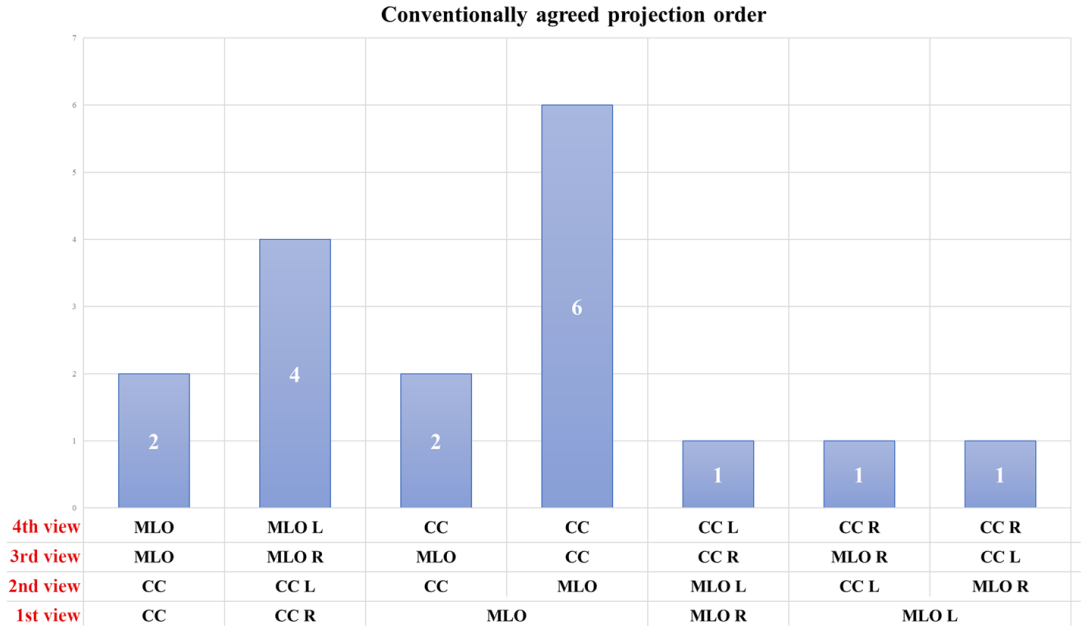

Figure 9: Graphical summary of conventionally agreed view acquisition orders for contrast-enhanced spectral mammography: CC craniocaudal view, MLO mediolateral oblique view, L left, R right. From Zanardo et al. Insight into Imaging. 2019

Among the 22 acquisition sequences (coming from 20 institutions) centred on the presence of previous suspect or clearly pathologic findings, we found substantial variability between different orders of acquisition, as shown in **Figure 10**. However, the most common sequence, adopted by 4/22 (19%) research groups, was:

1) CC, suspected side;

2) CC, non-suspected side;

3) MLO, suspected side;

4) MLO, non-suspected side.

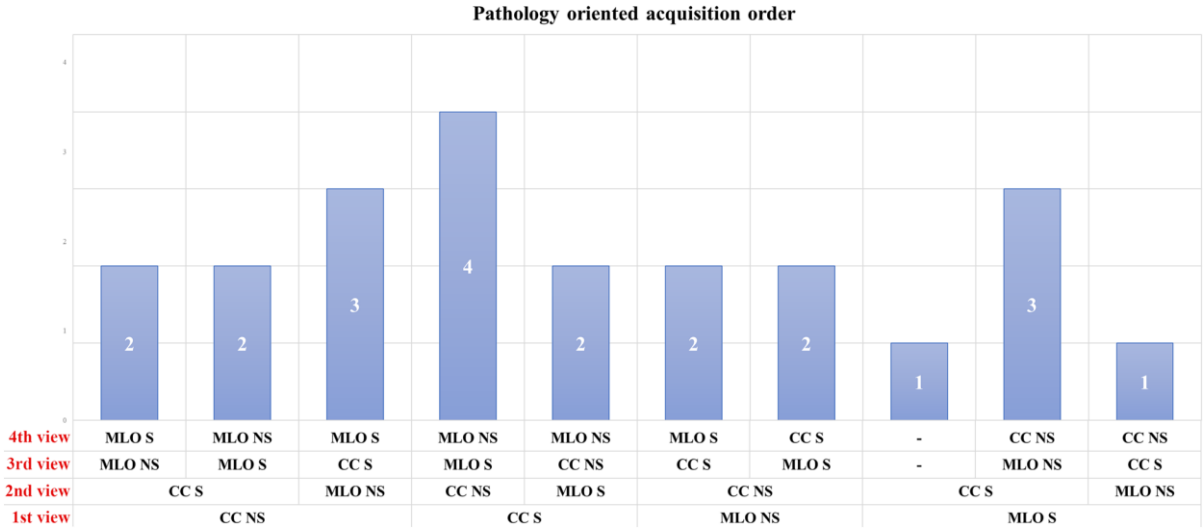

Figure 10: Graphical summary of pathology-oriented view acquisition orders for contrast-enhanced spectral mammography: CC craniocaudal view, MLO mediolateral oblique view, S suspicious breast, NS not suspicious breast. From Zanardo et al. Insight into Imaging. 2019

Contrast medium adverse reaction rate meta-analysis

Regarding side effects from contrast administration, 48/84 studies (57%) declared a preventive anamnestic screening for previous adverse reactions or general contraindications to ICM administration. Pre-examination tests of renal function was mentioned in 39/84 studies (46%). Of note, 14/84 studies (29%) reported 30 adverse reactions out of 14,012 patients, of which 26/30 (87%) were mild reactions limited to pruritus, hives, "scratchy throat", or other minor skin flushing that resolved promptly even when antihistamines or corticosteroids were not administered. In 3/30 (10%) cases (112,116,147), side effects were of moderate importance with nausea and vomiting, widespread urticaria resolved only after antihistamines and corticosteroids *per os*, and dyspnea that equally responded to oral antihistamine administration. Only 1/30 (3%) severe adverse reaction, requiring "intensive care" but resolved after short time, occurred in 14,012 patients (0.007%) (119).

Therefore, the number of adverse reactions related to ICM administration ranged from 0, reported by 70 (88%) studies, to a maximum number of 6 adverse reactions (75) with a total number of 30 adverse reactions, showing no heterogeneity (Q=64, degree of freedom 83, τ=2.0972, I^2=0%, P

= 0.931). As shown in the forest plot of **Figure 11**, using fixed-effect model, the pooled rate of adverse reactions across studies was 0.82%, with 0.64% and 1.05% as 95% CI.

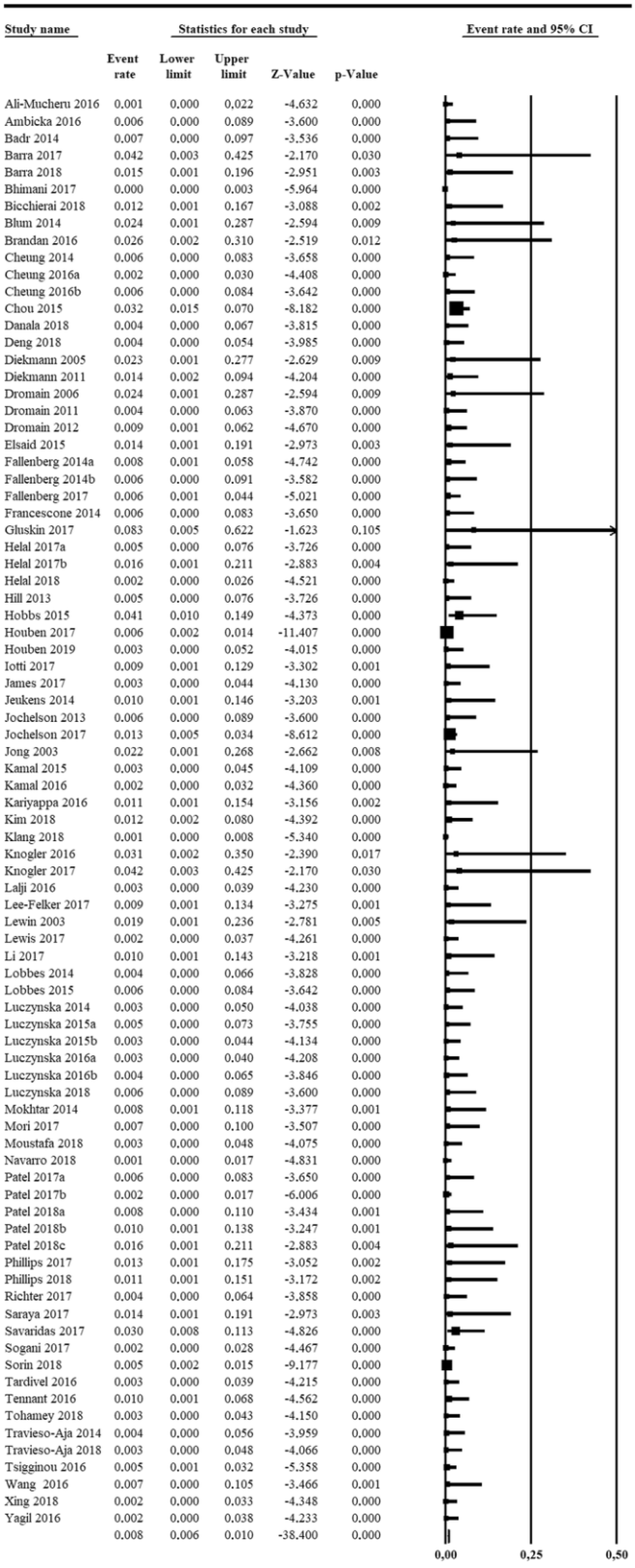

Figure 11: Forest plot of the 84 analysed articles on contrast-enhanced spectral mammography. No heterogeneity was found among studies (I^2 = 0%). The last row shows the pooled rate for adverse

reactions arising from ICM administration, calculated using the fixed-effect model. From Zanardo et al. Insight into Imaging. 2019

Visually inspecting the funnel plot in **Figure 12**, risk of publication bias was found, as confirmed by the Egger test (P = 0.00028).

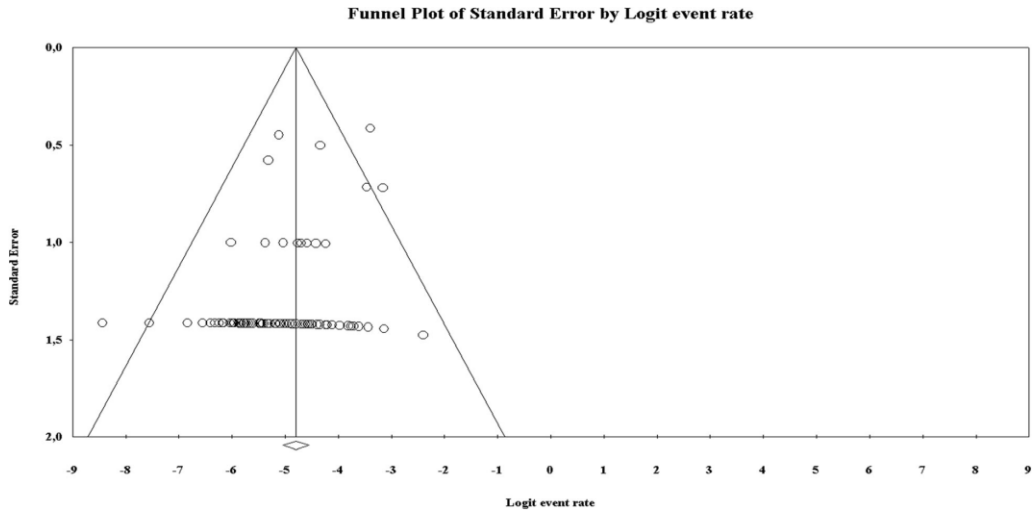

Figure 12: Funnel plot showing risk of publication bias in articles on contrast-enhanced spectral mammography, confirmed by the Egger test (P < 0.001). From Zanardo et al. Insight into Imaging. 2019

Discussion CESM systematic review

Our systematic review included 84 articles, accounting for 14,012 patients, reporting the use of CESM in various settings. The sheer number of studies and, as depicted in **Figure 13**, their increase in the last three years (27 studies between 2003 and December 2015, 57 from January 2016 to January 2019) points out a considerable interest in this emerging breast imaging modality.

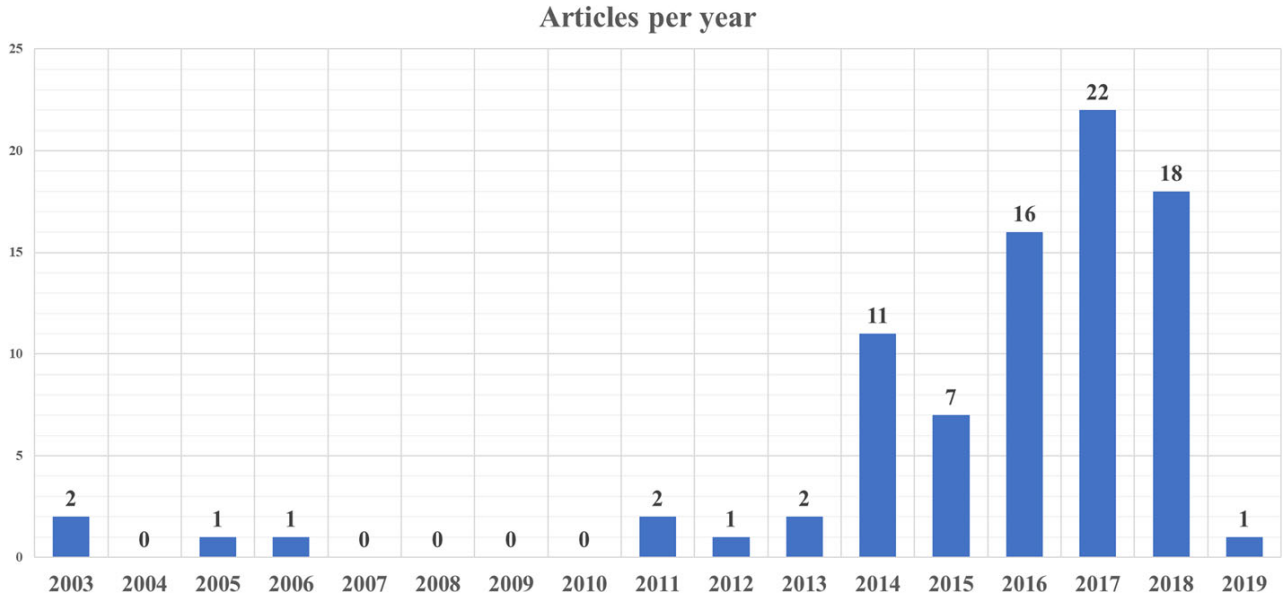

Figure 13: Graphic showing the number of articles published per year regarding contrast-enhanced spectral mammography. From Zanardo et al. Insight into Imaging. 2019

A number of narrative reviews (67,100,163–166) favourably outlined CESM future perspectives in several clinical settings (*e.g.*, recall work-up, preoperative staging, and monitoring the effect of neoadjuvant therapy) as a potential alternative to MRI.

In the first phase of CESM development, some non-fixed parameters regarding contrast medium administration (*i.e.*, contrast medium molecule, concentration, dose, flow rate, and injection modality) and some acquisition features (*i.e.*, time between contrast injection and first acquisition, kVp ranges for low- and high-energy acquisitions) gained an international agreement. However, in the framework of comprehensive optimisation and standardization of CESM, large-scale studies are undoubtedly needed to address the knowledge gap concerning the choice of technical parameters.

Our data show a consensus (93%) on the choice of 1.5 mL/kg contrast dose administered with a 3 mL/s flow rate (74%) and a less extensive agreement on the use of Iohexol (53% of all studies) at a concentration of 350 mg iodine/mL (30% of all studies). However, these parameters have probably been empirically adopted from CT protocols, as the first investigators plainly stated (68), without any other particular explication or justification. No dose-finding studies have been published yet.

Similarly, the common use of a power contrast injector (87% of all studies, with the remaining 13% coming from a single research group) is assumed from CT and MRI protocols in which it has been demonstrated to be effective in obtaining a stable contrast inflow and bolus shape (167–169). Moreover, the use of a power injector allows for the administration of a bolus chaser, reported only in 42% of all articles, a technical refinement that has shown good results in CT (170,171).

Two other points need to be mentioned. The first one is the correlation between menstrual cycle phase and CESM, for both background parenchymal enhancement, explored in a few studies (71,134,140), and for fluctuations of lesion contrast uptake. Secondly, since CESM is based on a dual x-ray exposure, of which the low-energy one has been demonstrated to be equal to standard DM (125), an increase in radiation dose is expected. However, while preliminary studies estimated a negligible (68) or curtailed AGD increase, studies specifically devised to ascertain CESM effective AGD found a substantial AGD increment ranging 42%–80% (114,118,142). While CESM AGDs remain under the threshold stated by European guidelines for screening mammography (172), further studies are needed to systematically compare AGD between different units and different vendors, an aspect which was only preliminary explored (114,142), further studies are needed to investigate CESM AGD.

Furthermore, we remark the absence of standardized protocols. This methodological void, especially regarding the acquisition workflow, represents a threat to reproducibility and comparison of imaging results. While 98% of all studies reporting the total examination time completed the examination before 10 min from contrast administration, and while some studies presented evidence

on the irrelevance of the acquisition order (113,123), there are no studies comparing different approaches.

The pooled rate of adverse reactions to ICM administration was 0.82% (0.64%–1.05% 95% CI) with a total of 30 adverse reactions in 14,012 patients, a rate similar to that reported for CT: 0.6% (173) in 84,928 adult patients or 0.7% (174) in 29,508 patients (given Iopromide, which is also used for CESM). Particularly, considering only severe adverse reactions in CT, Wang et al. (173) reported 11/84,928 (0.0129%) reactions, as well as Mortelé et al. (174) 4/29,508 (0.0135%). These rates seem to be higher than that found in our meta-analysis 1/14,012 (0.007%), a comparison to consider with caution due to the nature of rare events such as severe reactions to ICM. One aspect to consider is the different profile of patients undergoing CESM compared to those requiring contrast-enhanced CT, the former being that of basically "healthy" subjects, the latter implying the possibility of relevant disease, including also serious emergency conditions.

This review has limitations. Patient data are probably shared and duplicate among some studies from the same research group. This has been shown to negatively impact on review quality (175,176) and could only be prevented via individual patient data sharing (177). However, for technical aspects of this systematic review, our choice to evaluate study groups rather than single articles, should have mitigated this bias. Conversely, our pooled rate of adverse reactions could be underestimated.

In conclusion, our review shows that CESM is unevenly performed across different centres, in terms of contrast medium type and concentration and order of view acquisition. However, most research groups performed CESM using a contrast dose of 1.5 ml/kg, factory-set kVp ranges for low- and high-energy acquisitions, beginning image acquisition after 120 s from contrast medium injection and completing the examination within 10 minutes. Further studies are needed to investigate the role of background parenchymal enhancement and to harvest data that can firmly back up subsequent technical guidelines and consensus statements for standardized CESM protocols.

SECTION II: GADOLINIUM-BASED CONTRAST AGENT

This section is based on:

- *Zanardo et al. Technique and protocols for cardiothoracic time-resolved contrast-enhanced MRA sequences: a systematic review. Under review on Journal of Thoracic Imaging.*

Introduction

Gadolinium chelates are widely used as contrast media for MRI. The approved gadolinium-based contrast agent (GBCAs) have been considered safe and well tolerated from 1985 up until 2006. However, in recent years an association between GBCA administration and the development of nephrogenic systemic fibrosis (NSF) has been recognized in patients with severe renal impairment. This has led to modifications in clinical practice (178). Newer reports have emerged regarding the accumulation of gadolinium in bone, brain, and kidneys of patients who have no renal impairment. Evidence about gadolinium accumulation after multiple injections of GBCA does exist since a decade, early described in bone using mass spectroscopy on hip specimens taken during hip replacement surgery (179). Only in the last three years, gadolinium accumulation become a hot topic, especially for intracranial structures.

First evidence of this deposition in brain were reported by Kanda et al. (180) and Errante et al. (181), and later confirmed by different groups (169,180,182–187). Evaluating T1-weighted images in some brain structures, these authors found a statistically significant increase in signal intensity after repeated GBCA administrations, not only in dentate nucleus, but also in globus pallidus and in other brain regions.

In a recent paper on animal model (169), five different types of GBCAs (both linear and macrocyclic) were injected with a very high dose (25 times the standard dose) for 24 consecutive days. While increased signal intensity in T1-weighted images was seen for linear GBCAs, no difference was described for macrocyclic GBCAs. Some authors questioned about a threshold dose of GBCA needed to have a substantial increase in signal intensity, with a minimum number of 4 to 6 GBCA administrations (187).

Following a distribution model described by Hirano and Suzuki (188), the distribution of GBCAs can be simplified in a three-compartment model, consisting in plasma pool, interstitial fluid pool and bone. However, we do not know if gadolinium deposition is associate with deposition of the chelate or of the ion, alone or maybe bonded to an endogenous molecule such as calcium carbonate

or proteins (189). Despite the attempts to find a deposition mechanism have failed, studies (190,191) underline undoubtedly how an amount of gadolinium dissociates from the binding chelates, independently from the chemical structure of the GBCA.

Considering the recent debate on deposition/retention of gadolinium in the brain and other tissue (180), and that the Pharmacovigilance and Risk Assessment Committee of the European Medicines Agency recommended suspension of marketing authorization for four linear gadolinium GBCAs, this PhD section aimed towards a systematically review on technical protocols of time-resolved sequences, a cardiac MRI applications in which GBCA injection plays a crucial role, focusing on GBCA protocols, adopted technical parameters, and acquisition schemes.

4. Technique and protocols for cardiothoracic time-resolved contrast-enhanced MRA sequences: a systematic review

Introduction TR-MRA systematic review

Time resolved (TR), contrast-enhanced magnetic resonance angiography (MRA) techniques can be used for the assessment of the temporal dynamics of blood flow (192) and offer an alternative method to traditional contrast-enhanced techniques for high-quality MRA studies (193). Traditional contrast-enhanced MRA techniques are obtained acquiring images at a single point in time after GBCA injection, while TR-MRA sequences are obtained acquiring a series of images displaying the passage of the contrast bolus.

TR-MRA sequences are mostly known under commercial acronyms such as: *TRICKS* (Time-Resolved Imaging of Contrast KineticS) adopted by General Electric; *TWIST* (Time-resolved angiography With Stochastic Trajectories) by Siemens; *4D-TRAK* (4D Time-Resolved Angiography using Keyhole) or *CENTRA* (Contrast-Enhanced Timing Robust Angiography) by Philips; *TRAQ* (Time-Resolved AcQuisition) by Hitachi; *Freeze Frame* by Toshiba (194).

TR-MRA sequences are most often used to assess the heart and great thoracic vessels, and they find one of their main applications in the assessment of congenital heart diseases (CHD), where a comprehensive assessment of cardiovascular anatomy is paramount for both interventional planning and follow-up (195–198). Nevertheless, TR-MRA sequences are also widely used in different anatomical settings such as cerebral perfusion (199,200), spinal vascular disease (201), supra-aortic arteries (202), carotids (203), breast vessels (204), peripheral vascular anomalies (205), lower extremities (206). Moreover, TR-MRA is a potential tool that may aid successful central venous access in challenging patients (207).

Accurate timing of bolus arrival is not required, and, compared to traditional CE-MRA, reduced GBCA doses are required (208,209). Considering the recent debate on deposition/retention of gadolinium in the brain and other tissue (180), and that the Pharmacovigilance and Risk Assessment

Committee of the European Medicines Agency recommended suspension of marketing authorization for four linear gadolinium GBCAs (gadodiamide (Omniscan), gadoversetamide (OptiMARK), gadopentetate dimeglumine (Magnevist), and gadobenate dimeglumine (Multihance)) (210), recent efforts are aiming towards an attempt to reduce GBCA doses (211,212). Thus, TR-MRA could be more promising than traditional CE-MRA in this pursuit.

Thus, our aim was to review current cardiothoracic applications of TR-MRA sequences, focusing on GBCA protocols, adopted technical parameters, and acquisition schemes, to establish the range differences between acquisition protocols. This evidence will be of use to support a standardised approach to the imaging of vascular structures using a TR-MRA sequences.

Materials and methods TR-MRA systematic review

Study protocol

Institutional ethics approval was not required for this systematic review. The study protocol was registered on PROSPERO (https://www.crd.york.ac.uk/prospero/), the international prospective register of systematic reviews. The systematic review was reported according to the Preferred Reporting Items for Systematic reviews and Meta-Analyses (PRISMA) statement (106).

Search strategy and eligibility criteria

In May 2019, a systematic search was performed using PubMed (MEDLINE), EMBASE (Elsevier) and the Cochrane Library (Cochrane Database of Systematic Reviews, Cochrane Central Register of Controlled Trials) for articles that reported or may have potentially reported the use of TR-MRA sequences.

The search string used on EMBASE was: (twist OR 'twist sequence' OR tricks OR 'time resolved imaging of contrast kinetics'/exp OR 'time resolved angiography with stochastic trajectories' OR '4d trak' OR '4d time-resolved angiography using keyhole' OR traq OR 'time-resolved acquisition') AND ('nuclear magnetic resonance imaging'/exp OR 'mri' OR 'nmr imaging' OR 'imaging, magnetization transfer' OR 'magnetic resonance imaging' OR 'magnetic resonance tomography' OR 'magnetization transfer imaging' OR 'mr imaging' OR 'nuclear magnetic resonance imaging' OR 'magnetic resonance angiography'/exp OR 'mr angiography' OR 'mri angiography' OR 'nmr angiography' OR 'angiography, magnetic resonance' OR 'magnetic resonance angiography' OR 'nuclear magnetic resonance angiography' OR 'cardiovascular magnetic resonance'/exp OR 'cmr (cardiovascular magnetic resonance)' OR 'cardiac mri' OR 'cardiac magnetic resonance' OR 'cardiac magnetic resonance imaging' OR 'cardiovascular mri' OR 'cardiovascular magnetic resonance' OR 'cardiovascular magnetic resonance imaging') AND ('contrast medium'/exp OR 'contrast agent' OR

'contrast dye' OR 'contrast material' OR 'contrast media' OR 'contrast medium' OR 'radiocontrast medium' OR 'radiography contrast medium' OR 'roentgen contrast medium').

The search was limited to original articles, published in English, on peer-reviewed journals, and with an available abstract. Studies in vitro or on animal models were excluded. No limits were applied to publication date.

The initial screening of eligible articles was performed by two independent researchers (M.Z. and C.B.M. with 3- and 2-year experience in MRI), based solely on title and abstract content. Articles were considered eligible when reporting the use of TR-MRA sequences in the title or abstract, or when potentially containing such data in the manuscript. After downloading eligible articles, each full text was read for a complete assessment. Lastly, references of included articles were manually searched to check for further eligible studies. The same researchers who performed the literature search extracted all data independently and disagreements were resolved by consensus.

For each analysed article, year of publication, study design, number of patients and cardiovascular pathologies were retrieved. Moreover, magnetic field strength, device vendor, type and dose of CA, as well as injection modality, and TR-MRA sequences technical parameters were extracted.

Descriptive statistics were reported for all studies included in this review.

Results TR-MRA systematic review

Included studies

A flowchart of study selection is shown in **Figure 14**.

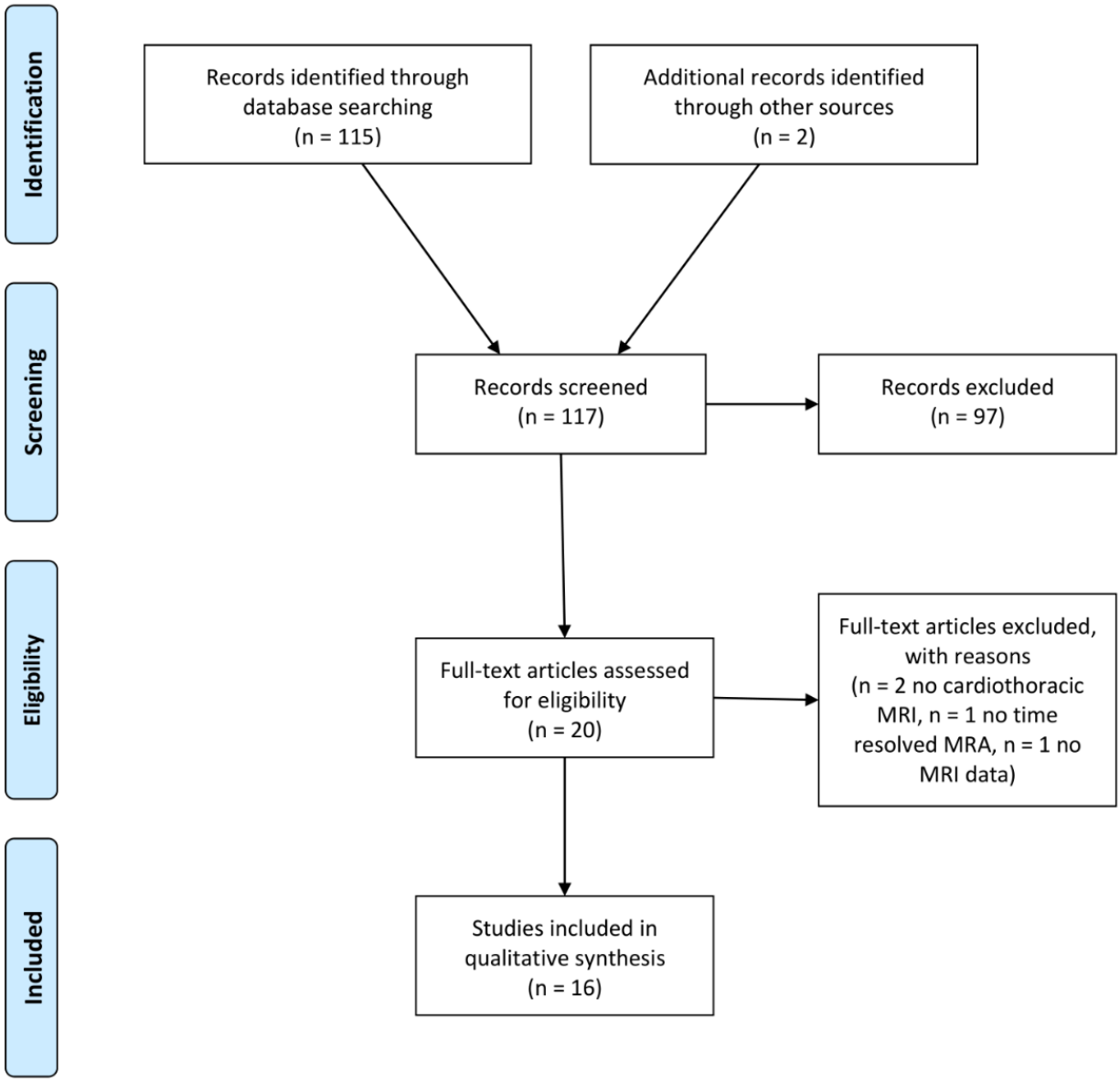

Figure 14: Flow chart of the literature study selection. From 117 initially retrieved articles, 16 were analysed.

Of 115 records identified through search query and 2 identified through other sources, 97 were excluded from title and abstract screening, and the remaining 20 were downloaded for full assessment. Finally, a total of 16 articles met the inclusion criteria (192,193,220–225,207,213–219).

All included papers were published between 1997 and 2019. Study design was prospective in 9/16 (56%) articles and retrospective in 7/16 (44%).

Study population ranged from 5 (220) to 185 (218), with a median number of subjects equal to 21 and an interquartile range (IQR) of 15–28 subjects, corresponding to a total of 506 enrolled or retrospectively selected individuals. A single article retrospectively analysed six healthy volunteers (219), while all other included subjects presented with a variety of cardiovascular pathologies: CHD or vessel anomalies, coronary artery disease, atrial fibrillation, or lung disease.

The magnetic field strengths documented were 1.5-T for 13/16 (81%), and 3-T for 3/16 (19%) (218,220,222) of the articles. MRI vendors were Siemens in 13/16 (81%) articles, General Electric in 2/16 (13%) and Philips in 1/16 (6%). The TR-MRA sequences employed were TWIST in 13/16 articles (81%), TRICKS in 2/16 articles (13%) (217,218), and CENTRA in 1/16 articles (6%) (214). The administered CA was gadobutrol (Gadovist) in 6/16 (38%) articles (192,207,216,222–224), gadopentetate dimeglumine (Magnevist) in 5/16 articles (31%) (193,213,214,218,220), gadobenate dimeglumine (Multihance) in 2/16 articles (13%) (217,219), gadodiamide (Omniscan) in 2/16 articles (13%) (215,225), and gadofosveset trisodium (AblavarTM) in 1/16 articles (6%) (221), as shown in **Figure 15**.

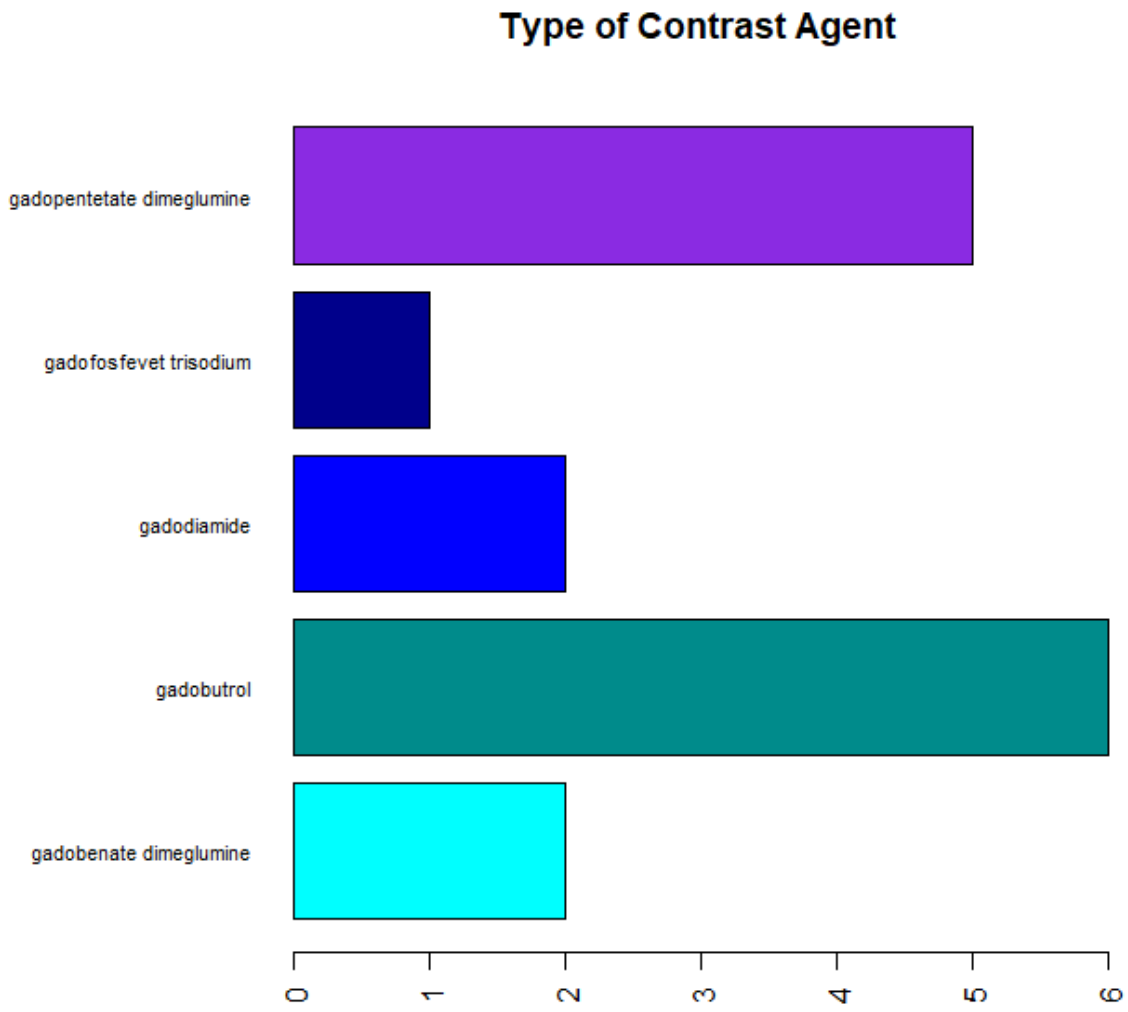

Figure 15: Bar chart showing gadolinium-based contrast agent used in the 16 analysed articles.

The CA dose was highly variable: several articles (192,215,216,218,222,225) used a fixed CA dose ranging from 2 mL (222) to 5 mL (192,216) for gadobutrol (Gadovist) (1.0 M) and ranging from 5 mL (225) to 12 mL (218) for the remaining CAs (0.5 M), while the other articles (193,207,213,214,217,219–221,223,224) utilized a dose based on patient body weight, which ranged from 0.02 mmol/kg (219,220) to 0.2 mmol/kg (214).

The CA was administered at a flow rate ranging from 1 mL/s (214) to 5 mL/s (221), and the same flow rate was used for saline flush, administered in volumes ranging between 10 mL (221) to

30 mL (215). Across the included literature all source TR-MRA sequences datasets were subtracted using an unenhanced contrast “mask” image.

Detailed information on MRI protocols and sequence parameters are provided in **Tables 7** and **8**.

Table 7: Main characteristics of MRI protocols of 16 analysed articles.

Author, year of publication	Study design	Pathology	Patients	B0 (T)	MRI Vendor	Contrast agent	CA Dose (mmol/kg)	Flow rate (mL/s)	Saline flush (mL)	TR-MRA Sequence
Sugrue, 2019	P	Congenital heart disease	21	1.5	Siemens	gadobutrol	0.1	3	20	TWIST
Obara-Moszynska, 2018	P	Turner syndrome	41	1.5	Siemens	gadobutrol	0.1	3.5	20	TWIST
Zghaib, 2018	R	Atrial fibrillation	50	1.5	Siemens	gadopentetate dimeglumine	0.2	5	20	TWIST
Armstrong, 2016	R	Difficult central venous access	15	1.5	Siemens	gadobutrol	0.1	2		TWIST
Wetzl, 2016	R	Aortic pathologies	11	3	Siemens	gadobutrol	2 mL	3		TWIST
Rapacchi, 2015	R	Thoracic vascular pathologies	5	3	Siemens	gadopentetate dimeglumine	0.02			TWIST
Rustogi, 2015	R	Atrial fibrillation	21	1.5	Siemens	gadofosveset trisodium	0.03	5	10	TWIST
Rapacchi, 2014	R	Healthy	6	1.5	Siemens	gadobenate dimeglumine	0.02			TWIST
Speiser, 2013	P	Tricuspid valve regurgitation	185	3	General Electric	gadopentetate dimeglumine	12 mL	2	25	TRICKS
Vogt, 2013	P	Congenital heart disease	26	1.5	Siemens	gadobutrol	5 mL	3	20	TWIST
Faggioni, 2012	P	Atrial fibrillation	33	1.5	General Electric	gadobenate dimeglumine	0.1	3	20	TRICKS
Seng, 2010	P	Coronary artery disease	20	1.5	Siemens	gadobutrol	5 mL	3	20	TWIST
Nael, 2009	R	Thoracic vascular pathologies	20	1.5	Siemens	gadodiamide	6 mL	2	30	TWIST
Krishnam, 2008	P	Thoracic vascular pathologies	13	1.5	Siemens	gadodiamide	5 mL	3	20	TWIST
Goo, 2007	P	Congenital heart disease	15	1.5	Philips	gadopentetate dimeglumine	0.2	1-3	0.2 mmol/kg	CENTRA
Hennig, 1997	P	Lung pathology	24	1.5	Siemens	gadopentetate dimeglumine	0.1			TWIST

P: prospective, R: retrospective; CA: contrast agent; TR-MRA: time-resolved magnetic resonance angiography; TWIST: Time-resolved angiography With Stochastic Trajectories; TRICKS: Time-Resolved Imaging of Contrast KineticS; CENTRA: Contrast-Enhanced Timing Robust Angiography.

Table 8: Main characteristics of time-resolved MRA sequence parameters of 16 analysed articles.

Author, year of publication	TR (ms)	TE (ms)	FA (°)	Bandwidth (Hz/pixel)	Slice thickness (mm)	Number of slices	FOV (mm^2)	Matrix	Voxel size	Time resolution (s per frame)	Parallel acquisition technique	N. series
Sugrue, 2019	2.87	1.17	25		2	64	500x340	512x358	1.4x1.0x2			10
Obara-Moszynska, 2018	2.3	0.87			1.5		500x310	384x224	1.4x1.3x1.5	3-5		
Zghaib, 2018	2.2	0.9	24		1.5					6.1	GRAPPA	13
Armstrong, 2016	2.56	0.91	25		1.5	96	500				GRAPPA	8
Wetzl, 2016	2.89	1.05	17	570	1.2	73	333x380	269x384	1.2x1.0x1.2	2.4	GRAPPA	
Rapacchi, 2015	2.6	1	25		3-6				1.1x1.1x3-6	2.35		
Rustogi, 2015	1.6	0.8	30	900	1.0-1.5	70		256x192	2.0x1.5	3-4	GRAPPA	10-12
Rapacchi, 2014	2.3	0.97	25	800	1.3-2.2	64-96		512x270-294		5.9		
Speiser, 2013	3.5	1.3		83.3 kHz	5.8		440x396	256x160				
Vogt, 2013	2.66	1.07	25	650	1.5	88	400x300	384x230	1.3x1.0x1.5	4.1	GRAPPA	15
Faggioni, 2012	3.4	1.3	35	83 kHz	3	52-60		320x224		3.5-3.8		8
Seng, 2010	2.7	1.05	25			96	400	320x266	1.5x1.3x2.1	4.3	GRAPPA	14
Nael, 2009	2	0	20	1000			500x458	384x342	1.3x.13x7			20
Krishnam, 2008	2.57	1.06	25	750	3		450x1000	256x512	1.2x1x3	1.2	GRAPPA	24
Goo, 2007	3.9	1.3	30		1.6	50	512x384-156	512x384-156	0.7x1.1x1.6-0.5x0.5x0.8		SENSE	10
Hennig, 1997	3.4	1.4	40	780		40-60		256				

TR: repetition time; TE: echo time; FA: flip angle; FOV: field of view; GRAPPA: GeneRalized Autocalibrating Partial Parallel Acquisition; SENSE: SENSitivity Encoding.

Discussion TR-MRA systematic review

In this systematic review, we investigated the cardiothoracic applications of TR-MRA sequences, focusing on technical aspects and contrast medium protocols.

Upon review of the publications the TR-MRA sequence appeared to not have changed substantially over time (**Table 8**) and the 16 papers dating from 1997 to 2019 reported comparable parameters and were deemed appropriate for inclusion. The existing evidence base reflects the complexity of this sequence, which is image intensive and has limited clinical application (226,227). Its specialized focus is evident in the small patient cohorts reported in the literature (**Table 8**).

TR-MRA sequences represent one of the most promising imaging modalities for applications in non-invasive vascular imaging, including simultaneous anatomic and functional analysis of many vascular pathologies including arterio-venous malformations (228). Moreover, TR-MRA is a powerful tool for investigating paediatric and adult CHD, still faring better than non-contrast MRA, especially considering the long acquisition times of the latter, which are often poorly compatible with imaging younger patients (229,230).

Data was principally acquired at a magnet field strength of 1.5-T and various factors would have influenced this, most likely the fact that cardiac scans at 3-T are susceptible to banding artefacts (231). **Table 7** identifies the majority of studies were performed as part of a dedicated cardiac examination predominantly employing 1.5-T. Whilst literature shows higher signal to noise ratio which can translate into higher spatial resolution at 3-T, due to artefact issues during cardiac imaging this is less relevant (231–233).

The systematic review identified a range of contrast mediums employed over time. Approved gadolinium-based CAs were considered safe and well tolerated from 1985 up until 2006 (234). However, in recent years an association between GBCA administration and the development of nephrogenic systemic fibrosis (NSF) has been recognized in patients with severe renal impairment (235). This led to modifications in clinical practice (178). Precautionary measures instigated in 2006 to mitigate against the risk of NSF by restricting the use of linear chelate of GBCA in patients with

impaired renal function and using lower doses of macrocyclic chelate GBCAs to achieve diagnostic-quality studies the incidence of NSF has ceased. The review aligned to the limited use of gadodiamide (Omniscan) from 2010 due to its association with development of NSF in patients with reduced renal function, as no literature beyond 2009 stated its use (236,237). Five different chelates were identified across the included articles as being administered for cardiothoracic TR-MRA, namely: gadobutrol (Gadovist), gadopentetate dimeglumine (Magnevist), gadobenate dimeglumine (Multihance), gadodiamide (Omniscan), and gadofosveset trisodium (AblavarTM). It is well established that concentration and relaxivity of contrast mediums affect image quality in contrast-enhanced MRA (238), gadobutrol (Gadovist), the most commonly used contrast medium throughout our review, 6/16 (38%) (192,207,216,222–224) articles, has a relatively higher T1-relaxivity than gadopentetate dimeglumine (Magnevist) and gadodiamide (Omniscan) (239), but lower than that of gadobenate dimeglumine (Multihance) and gadofosveset trisodium (AblavarTM) (**Table 9**) (238,240,241).

Table 9: Main characteristics of gadolinium-based contrast agent used for cardiothoracic applications in our review. r1 and r2 relaxivities for included gadolinium-based contrast agents obtained in plasma at 37°C at 1.5T (data from Rohrer et al.). Contrast mediums with the larger relaxivities are those with higher molecular weights, higher protein bonding, or both.

Short name	Generic name	Trade name	Chemical structure	T1 Relaxivity (L/mmol-s) at 1.5T	T2 Relaxivity (L/mmol-s) at 1.5T	T1 Relaxivity (L/mmol-s) at 3T	T2 Relaxivity (L/mmol-s) at 3T	Molarity (M)	Standard dose (mmol/kg)	Maximum dose (mmol/kg)
Gd-DO3A-butrol	gadobutrol	Gadovist	Macrocyclic	5.2	6.1	5.0	7.1	1.0	0.1	0.2
Gd-DTPA	gadopentetate dimeglumine	Magnevist	Linear	4.1	4.6	3.7	5.2	0.5	0.1	0.2
Gd-BOPTA	gadobenate dimeglumine	Multihance	Linear	6.3	8.7	5.5	11.0	0.5	0.1	0.2
Gd-DTPA-BMA	gadodiamide	Omniscan	Linear	4.3	5.2	4.0	5.6	0.5	0.1	0.2
MS-325	gadofosveset trisodium	AblavarTM	Linear	19	34	9.9	60.0	0.25	0.03	0.05

As stated in the introduction section, in March 2017, mainly due to evidence of brain gadolinium deposition in brain tissue, most notably in the dentate nuclei and globus pallidus (242), the European Medicines Agency fully suspended the use of gadofosveset trisodium, gadopentetate

dimeglumine (Magnevist), gadobenate dimeglumine (Multihance) and gadodiamide (Omniscan) from the market for safety reasons and only gadobutrol (Gadovist) is actually available on the market for cardiothoracic TR-MRA sequences (242). However, considering that CHD patients necessitate serial contrast enhanced cardiac MRI as part of their clinical workflow, the several GBCA injections may lead to increased risk gadolinium deposits. In this context, it is crucial to reduce and optimise, where possible, the GBCA dose, being gadolinium depositions on yet unclear clinical significance and unresolved if the gadolinium deposit is dose-dependent (242–244).

The use of the more concentrated (1.0 M) agent gadobutrol (Gadovist), which also has a slightly higher relaxivity, permits the use of half the volume to achieve a comparable dose (245). It has been suggested that this lower volume may result in a more well-defined bolus with a sharper peak (246). In an animal model, a more compact bolus shape was observed after administration of gadobutrol (Gadovist) compared with gadopentetate dimeglumine (Magnevist) in minipigs, while first-pass imaging characteristics of gadofosveset trisodium (AblavarTM) and gadobenate dimeglumine (Multihance) are equally well suited for first pass TR-MRA at 3-T (247). This was demonstrated in MRA, where contrast medium concentration, relaxivity and image-acquisition techniques, play an essential role: overall image quality was rated higher in examinations acquired injecting 1.0 M gadobutrol (Gadovist) than in those acquired with 0.5 M gadopentetate dimeglumine (Magnevist) (248). GBCAs are classified according to their chemical structure (linear or macrocyclic, **Table 9**) and the ionic or nonionic nature of the ligand (189). None of the studies included in our review administered gadoterate meglumine (gadoteric acid, Dotarem), although the newly FDA-approved macrocyclic GBCA and the high-molar gadobutrol (Gadovist) lead to a comparable image quality (249).

Our review showed a high heterogeneity among studies in terms MRI protocols reflecting the different strategies of contrast medium injection modality: fixed dose (2–5 ml for gadobutrol (Gadovist) (1.0 M) or 5–12 for other GBCA (0.5 M)) or based on patient body weight (0.02–0.2 mmol/kg). The 0.02 mmol/kg low dose was adopted by only one research group that published two

different studies (219,220). The tenfold reduction in GBCA dose compared with the conventional 0.1-2 mmol/kg doses is noteworthy and aligns to a number of research studies that have demonstrated that administering GBCA based on patient body weight can lead to a reduction of the variability of signal intensity (46,250,251). GBCA dose tailoring would be most beneficial in order to avoid both administering too high a dose in underweight patients, as it could lead to increased chance of GBCA adverse events (252).

Theoretically, due to the lengthening in T1 times of tissues on 3T scans, it may be viable to reduce GBCA dose (253–255). However on the three 3-T studies included, two reported a fixed dose of gadobutrol (Gadovist) Wetzl et al. (222) 2 mL (1.0 M) and Speiser et al. (218) 12 mL (0.5 M) of gadopentetate dimeglumine (Magnevist), thus a threefold difference in dose was noted between the two studies, whilst Rapacchi et al. (220) administered a dose based on patient body weight equal to 0.02 mmol/kg of gadopentetate dimeglumine (Magnevist). This specifically low dose was however used to facilitate a further GBCA dose to acquire a higher resolution MRA sequence.

Concerning the mechanism of GBCA injection, protocol and flow rate are matters that require clarity in studies to facilitate an ability to compare studies. Injection flow rate was found to be predominately heterogenous among studies from 1 mL/s (214) to 5 mL/s (193,221). The impact of various injection methods was examined in a controlled setting in an animal model experiment (169). Budjan et al. (256) who demonstrated that automated injection provided a more defined bolus shape.

As stated previously literature has identified the value of TR-MRA in imaging CHD patients. Vogt et al. (192) and Krishnam et al. (225) demonstrated that TR-MRA yields robust images and added diagnostic value through dynamic acquisition in CHD patients or patients with vessel anomalies; Rustogi et al. (221) studied patients with atrial fibrillation, and described the role of TR-MRA for quantitative assessment of pulmonary venous anatomy. Zghaib et al. (193) described how TR-MRA offers better overall image quality, pulmonary veins visualization and similarly reproducible pulmonary veins measurements compared to traditional CE-MRA, without the challenges of proper bolus timing in pre-atrial fibrillation ablation pulmonary venous mapping.

Furthermore, Obara-Moszynska et al. (223) showed that cardiac measurements performed on TR-MRI and echocardiography were comparable in most patients with Turner syndrome. The literature indicates that the method of sequence application varies across centres, however no literature exists to explain the reason behind this variability and further research is recommended. The TR-MRA parameters and the contrast dose could be different if the target of TR-MRA are veins or arteries or both. Moreover, even in patients with CHD the anatomy and blood distribution are very different, i.e. in patients with single ventricle and Fontan circulation. In a recent paper Sugrue et al. (224) analysed 21 CHD patients, and demonstrated that a novel subtracted TR-MRA technique improved visualization of the pulmonary veins and left atrium compared to the source TR-MRA sequence and this indicates further work on the sequence may be valuable in isolating certain anatomical structures in these complex patients. The sequence has evolved to be relevant as an interventional option for patients requires central line access. TR-MRA enabled successful identification of candidate sites for central line access, as well as diagnosing complications of long-term access such as venous thrombosis or congenital venous anomalies in complex patients (207).

A lack of agreement between studies in utilizing either an absolute amount of contrast medium or per-kg of body weight dosage was evident. Considering the specialized use of this sequence over two decades there appears to be a paucity of published papers which does impact on the ability to identify potential trends in TR-MRA protocols.

Results showed that a variety of different technical approaches were adopted throughout different studies, highlighting a lack of standardization and consensus on this technique. In fact, even though TR-MRA sequences have been tested for a wide spectrum of indications, optimisation of these sequences does not limit to the selection of ideal pulse sequence parameters, but also to the application of dedicated contrast medium application protocols.

In conclusion, cardiothoracic applications of TR-MRA sequences are currently adopted in different clinical settings with different technical approaches, mostly due to different GBCA dose and

type. Further studies are warranted, in order to establish the appropriate parameters for TR-MRA, especially in relation to GBCA protocols.

Figures

References

1. Sardanelli F. Trends in radiology and experimental research. Eur Radiol Exp. 2017;1(1):1.
2. Bae KT. Intravenous contrast medium administration and scan timing at CT: considerations and approaches. Radiology. 2010;256(1):32–61.
3. FDA. Paving the way for personalized medicine: FDA's role in a new era of medical product development. US Food Drug Adm. 2013;1–61.
4. Chambers TP, Baron RL, Lush RM. Hepatic CT enhancement. Part I. Alterations in the volume of contrast material within the same patients. Radiology. 1994;193(2):513–517.
5. Bae KT, Heiken JP, Brink JA. Aortic and hepatic peak enhancement at CT: effect of contrast medium injection rate--pharmacokinetic analysis and experimental porcine model. Radiology. 1998;206(2):455–464.
6. Kim T, Murakami T, Takahashi S, et al. Effects of injection rates of contrast material on arterial phase hepatic CT. AJR Am J Roentgenol. 1998;171(2):429–432.
7. Heiken JP, Brink JA, McClennan BL, Sagel SS, Crowe TM, Gaines M V. Dynamic incremental CT: effect of volume and concentration of contrast material and patient weight on hepatic enhancement. Radiology. 1995;195(2):353–357.
8. Kormano M, Dean PB. Extravascular contrast material: the major component of contrast enhancement. Radiology. 1976;121(2):379–382.
9. Kormano M, Partanen K, Soimakallio S, Kivimäki T. Dynamic contrast enhancement of the upper abdomen: effect of contrast medium and body weight. Invest Radiol. 18(4):364–367.
10. Davenport MS, Parikh KR, Mayo-Smith WW, Israel GM, Brown RKJ, Ellis JH. Effect of fixed-volume and weight-based dosing regimens on the cost and volume of administered iodinated contrast material at abdominal CT. J Am Coll Radiol. 2017;14(3):359–370.
11. Yamashita Y, Komohara Y, Takahashi M, et al. Abdominal helical CT: evaluation of optimal doses of intravenous contrast material--a prospective randomized study. Radiology. 2000;216(3):718–723.

12. Awai K, Inoue M, Yagyu Y, et al. Moderate versus high concentration of contrast material for aortic and hepatic enhancement and tumor-to-liver contrast at multi-detector row CT. Radiology. 2004;233(3).

13. Awai K, Hiraishi K, Hori S. Effect of contrast material injection duration and rate on aortic peak time and peak enhancement at dynamic CT involving injection protocol with dose tailored to patient weight. Radiology. 2004;230(1):142–150.

14. Awai K, Hori S. Effect of contrast injection protocol with dose tailored to patient weight and fixed injection duration on aortic and hepatic enhancement at multidetector-row helical CT. Eur Radiol. 2003;13(9):2155–2160.

15. Yanaga Y, Awai K, Nakayama Y, et al. Pancreas: patient body weight tailored contrast material injection protocol versus fixed dose protocol at dynamic CT. Radiology. 2007;245(2):475–482.

16. Ichikawa T, Erturk SM, Araki T. Multiphasic contrast-enhanced multidetector-row CT of liver: contrast-enhancement theory and practical scan protocol with a combination of fixed injection duration and patients' body-weight-tailored dose of contrast material. Eur J Radiol. 2006;58(2):165–176.

17. Arana E, Martí-Bonmatí L, Tobarra E, Sierra C. Cost reduction in abdominal CT by weight-adjusted dose. Eur J Radiol. 2009;70(3):507–511.

18. Bae KT, Heiken JP, Brink JA. Aortic and hepatic contrast medium enhancement at CT. Part I. Prediction with a computer model. Radiology. 1998;207(3):647–655.

19. Kondo H, Kanematsu M, Goshima S, et al. Abdominal multidetector CT in patients with varying body fat percentages: estimation of optimal contrast material dose. Radiology. 2008;249(3):872–877.

20. Roubenoff R, Kehayias JJ. The meaning and measurement of lean body mass. Nutr Rev. 1991;49(6):163–175.

21. Morgan DJ, Bray KM. Lean body mass as a predictor of drug dosage. Implications for drug

therapy. Clin Pharmacokinet. 1994;26(4):292–307.

22. Ho LM, Nelson RC, Delong DM. Determining contrast medium dose and rate on basis of lean body weight: does this strategy improve patient-to-patient uniformity of hepatic enhancement during multi-detector row CT? Radiology. 2007;243(2):431–437.

23. Bae KT, Seeck BA, Hildebolt CF, et al. Contrast enhancement in cardiovascular MDCT: Effect of body weight, height, body surface area, body mass index, and obesity. Am J Roentgenol. 2008;190(3):777–784.

24. Yanaga Y, Awai K, Nakaura T, et al. Effect of contrast injection protocols with dose adjusted to the estimated lean patient body weight on aortic enhancement at CT angiography. Am J Roentgenol. 2009;192(4):1071–1078.

25. Kondo H, Kanematsu M, Goshima S, et al. Body size indexes for optimizing iodine dose for aortic and hepatic enhancement at multidetector CT: comparison of total body weight, lean body weight, and blood volume. Radiology. 2010;254(1):163–169.

26. Kondo H, Kanematsu M, Goshima S, et al. Aortic and hepatic enhancement at multidetector CT: evaluation of optimal iodine dose determined by lean body weight. Eur J Radiol. 2011;80(3):e273-7.

27. Onishi H, Murakami T, Kim T, et al. Abdominal multi-detector row CT: Effectiveness of determining contrast medium dose on basis of body surface area. Eur J Radiol. 2011;80(3):643–647.

28. Svensson A, Nouhad J, Cederlund K, et al. Hepatic contrast medium enhancement at computed tomography and its correlation with various body size measures. Acta Radiol. 2012;53(6):601–606.

29. Kidoh M, Nakaura T, Oda S, et al. Contrast Enhancement During Hepatic Computed Tomography: Effect of Total Body Weight, Height, Body Mass Index, Blood Volume, Lean Body Weight, and Body Surface Area. J Comput Assist Tomogr. 2013;37(2):159–164.

30. Kondo H, Kanematsu M, Goshima S, et al. Body size indices to determine iodine mass with

contrast-enhanced multi-detector computed tomography of the upper abdomen: Does body surface area outperform total body weight or lean body weight? Eur Radiol. 2013;23(7):1855–1861.

31. Prado CMM, Heymsfield SB. Lean Tissue Imaging: A New Era for Nutritional Assessment and Intervention. J Parenter Enter Nutr. 2014;38(8):940–953.
32. Nyman U. James Lean Body Weight Formula Is Not Appropriate for Determining CT Contrast Media Dose in Patients with High Body Mass Index. Radiology. 2016;278(3):956–957.
33. Caruso D, De Santis D, Rivosecchi F, et al. Lean body weight-tailored iodinated contrast injection in obese patient: Boer versus James formula. Biomed Res Int. 2018;2018:1–6.
34. Tao SM, Wichmann JL, Schoepf UJ, Fuller SR, Lu GM, Zhang LJ. Contrast-induced nephropathy in CT: incidence, risk factors and strategies for prevention. Eur Radiol. 2016;26(9):3310–3318.
35. Van Cauteren T, Honoria Da Silva E, Van Gompel G, et al. Iodine dose of administered contrast media affects the level of radiation-induced DNA damage during cardiac CT scans. Am J Roentgenol. 2019;1–6.
36. Hamer OW, Aguirre DA, Casola G, Lavine JE, Woenckhaus M, Sirlin CB. Fatty liver: imaging patterns and pitfalls. RadioGraphics. 2006;26(6):1637–1653.
37. WHO | Obesity and overweight. WHO. 2016;
38. Awai K, Kanematsu M, Kim T, et al. The optimal body size index with which to determine iodine dose for hepatic dynamic CT: a prospective multicenter study. Radiology. 2016;278(3):773–781.
39. DHSS/MRC Group on Obesity Research, James WPT, William PT, Waterlow JC, John C, et al. Research on obesity: a report of the DHSS/MRC group. 1976.
40. Boer P. Estimated lean body mass as an index for normalization of body fluid volumes in humans. Am J Physiol. 1984;247(4 Pt 2):F632-6.

41. Wang Y, Chen X, Song Y, Caballero B, Cheskin LJ. Association between obesity and kidney disease: A systematic review and meta-analysis. Kidney Int. 2008;73(1):19–33.
42. Taylor HL, Brozek J, Keys A, Carlson W. Basal cardiac function and body composition with special reference to obesity. J Clin Invest. 1952;31(11):976–983.
43. Janmahasatian S, Duffull SB, Ash S, Ward LC, Byrne NM, Green B. Quantification of lean bodyweight. Clin Pharmacokinet. 2005;44(10):1051–1065.
44. Hume R. Prediction of lean body mass from height and weight. J Clin Pathol. 1966;19(4):389–391.
45. Schulz KF, Altman DG, Moher D. CONSORT 2010 Statement: updated guidelines for reporting parallel group randomised trials. BMJ. 2010;340:c332–c332.
46. Zanardo M, Doniselli FM, Esseridou A, et al. Abdominal CT: a radiologist-driven adjustment of the dose of iodinated contrast agent approaches a calculation per lean body weight. Eur Radiol Exp. 2018;2(1):41.
47. Wolf LA. Giving the complete picture: why publishing negative results is important. J Emerg Nurs. 2017;43(3):289–290.
48. Matosin N, Frank E, Engel M, Lum JS, Newell KA. Negativity towards negative results: a discussion of the disconnect between scientific worth and scientific culture. Dis Model Mech. 2014;7(2):171–173.
49. van Daele PLA. Negative results worth publishing. Neth J Med. 2018;76(7):309.
50. Rewarding negative results keeps science on track. Nature. 2017;551(7681):414.
51. Nygaard I. The importance of publishing trials with negative results. Am J Obstet Gynecol. 2017;216(6):541–542.
52. Kondo H, Kanematsu M, Goshima S, et al. Body size indices to determine iodine mass with contrast-enhanced multi-detector computed tomography of the upper abdomen: does body surface area outperform total body weight or lean body weight? Eur Radiol. 2013;23(7):1855–1861.

53. Bellesi L, Wyttenbach R, Gaudino D, et al. A simple method for low-contrast detectability, image quality and dose optimisation with CT iterative reconstruction algorithms and model observers. Eur Radiol Exp. 2017;1(1):18.

54. Sun J, Hu D, Shen Y, et al. Improving image quality with model-based iterative reconstruction algorithm for chest CT in children with reduced contrast concentration. Radiol Med. 2019;

55. Laurent G, Villani N, Hossu G, et al. Full model-based iterative reconstruction (MBIR) in abdominal CT increases objective image quality, but decreases subjective acceptance. Eur Radiol. 2019;29(8):4016–4025.

56. Goshima S, Kanematsu M, Noda Y, et al. Determination of optimal intravenous contrast agent iodine dose for the detection of liver metastasis at 80-kVp CT. Eur Radiol. 2014;24(8):1853–1859.

57. Martens B, Hendriks BMF, Eijsvoogel NG, Wildberger JE, Mihl C. Individually Body weight–adapted contrast media application in computed tomography imaging of the liver at 90 kVp. Invest Radiol. 2019;54(3):177–182.

58. Walgraeve M-S, Pyfferoen L, Van De Moortele K, Zanca F, Bielen D, Casselman J. Implementation of patient-tailored contrast volumes based on body surface area harmonizes contrast enhancement and reduces contrast load in small patients in portal venous phase abdominal CT. Eur J Radiol. 2019;

59. Svensson A, Nouhad J, Cederlund K, et al. Hepatic contrast medium enhancement at computed tomography and its correlation with various body size measures. Acta radiol. 2012;53(6):601–606.

60. Pesapane F, Codari M, Sardanelli F. Artificial intelligence in medical imaging: threat or opportunity? Radiologists again at the forefront of innovation in medicine. Eur Radiol Exp. 2018;2(1):35.

61. Bae KT. Intravenous contrast medium administration and scan timing at CT: considerations

and approaches. Radiology. 2010;256(1):32–61.

62. Frigerio A, Sardanelli F, Podo F. Radiological screening of breast cancer: evolution. Breast Cancer. 2017. p. 171–203.

63. Pisano ED, Gatsonis C, Hendrick E, et al. Diagnostic performance of digital versus film mammography for breast-cancer screening. N Engl J Med. 2005;353(17):1773–1783.

64. Gilbert FJ, Tucker L, Young KC. Digital breast tomosynthesis (DBT): a review of the evidence for use as a screening tool. Clin Radiol. 2016;71(2):141–150.

65. Pattacini P, Nitrosi A, Giorgi Rossi P, et al. Digital mammography versus digital mammography plus tomosynthesis for breast cancer screening: the Reggio Emilia tomosynthesis randomized trial. Radiology. 2018;288(2):375–385.

66. Marinovich ML, Hunter KE, Macaskill P, Houssami N. Breast cancer screening using tomosynthesis or mammography: a meta-analysis of cancer detection and recall. JNCI J Natl Cancer Inst. 2018;110(9):942–949.

67. Patel BK, Lobbes MBI, Lewin J. Contrast enhanced spectral mammography: a review. Semin Ultrasound, CT MRI. 2018;39(1):70–79.

68. Jong RA, Yaffe MJ, Skarpathiotakis M, et al. Contrast-enhanced digital mammography: initial clinical experience. Radiology. 2003;228(3):842–850.

69. Diekmann F, Diekmann S, Jeunehomme F, Muller S, Hamm B, Bick U. Digital mammography using iodine-based contrast media. Invest Radiol. 2005;40(7):397–404.

70. Dromain C, Balleyguier C, Muller S, et al. Evaluation of tumor angiogenesis of breast carcinoma using contrast-enhanced digital mammography. Am J Roentgenol. 2006;187(5):W528–W537.

71. Hill ML, Mainprize JG, Carton A-K, et al. Anatomical noise in contrast-enhanced digital mammography. Part II. Dual-energy imaging. Med Phys. 2013;40(8).

72. Dromain C, Balleyguier C, Adler G, Garbay JR, Delaloge S. Contrast-enhanced digital mammography. Eur J Radiol. 2009;69(1):34–42.

73. Skarpathiotakis M, Yaffe MJ, Bloomquist AK, et al. Development of contrast digital mammography. Med Phys. 2002;29(10):2419–2426.

74. Bhimani C, Matta D, Roth RG, et al. Contrast-enhanced spectral mammography. Acad Radiol. 2017;24(1):84–88.

75. Chou C-P, Lewin JM, Chiang C-L, et al. Clinical evaluation of contrast-enhanced digital mammography and contrast enhanced tomosynthesis—Comparison to contrast-enhanced breast MRI. Eur J Radiol. 2015;84(12):2501–2508.

76. Tennant SL, James JJ, Cornford EJ, et al. Contrast-enhanced spectral mammography improves diagnostic accuracy in the symptomatic setting. Clin Radiol. 2016;71(11):1148–1155.

77. Lewis TC, Pizzitola VJ, Giurescu ME, et al. Contrast-enhanced digital mammography: a single-institution experience of the first 208 cases. Breast J. 2017;23(1):67–76.

78. Moustafa AFI, Kamal EF, Hassan MM, Sakr M, Gomaa MMM. The added value of contrast enhanced spectral mammography in identification of multiplicity of suspicious lesions in dense breast. Egypt J Radiol Nucl Med. 2018;49(1):259–264.

79. Saraya S, Adel L, Mahmoud A. Indeterminate breast lesions: can contrast enhanced digital mammography change our decisions? Egypt J Radiol Nucl Med. 2017;48(2):547–552.

80. Tardivel A-M, Balleyguier C, Dunant A, et al. Added Value of Contrast-Enhanced Spectral Mammography in Postscreening Assessment. Breast J. 2016;22(5):520–528.

81. Patel BK, Davis J, Ferraro C, et al. Value added of preoperative contrast-enhanced digital mammography in patients with invasive lobular carcinoma of the breast. Clin Breast Cancer. 2018;18(6):e1339–e1345.

82. Travieso-Aja M del M, Naranjo-Santana P, Fernández-Ruiz C, et al. Factors affecting the precision of lesion sizing with contrast-enhanced spectral mammography. Clin Radiol. 2018;73(3):296–303.

83. Helal MHH, Salem DSS, Salaleldin LAA, et al. The impact of contrast-enhanced spectral

mammogram (CESM) and three-dimensional breast ultrasound (3DUS) on the characterization of the disease extend in cancer patients. Br J Radiol. 2018;64(8).

84. Lee-Felker SA, Tekchandani L, Thomas M, et al. Newly diagnosed breast cancer: comparison of contrast-enhanced spectral mammography and breast MR imaging in the evaluation of extent of disease. Radiology. 2017;285(2):389–400.

85. Patel BK, Garza SA, Eversman S, Lopez-Alvarez Y, Kosiorek H, Pockaj BA. Assessing tumor extent on contrast-enhanced spectral mammography versus full-field digital mammography and ultrasound. Clin Imaging. 2017;46:78–84.

86. Helal MH, Mansour SM, Zaglol M, Salaleldin LA, Nada OM, Haggag MA. Staging of breast cancer and the advanced applications of digital mammogram: what the physician needs to know? Br J Radiol. 2017;90(1071).

87. Ambicka A, Luczynska E, Adamczyk A, Harazin-Lechowska A, Sas-Korczynska B, Niemiec J. The tumour border on contrast-enhanced spectral mammography and its relation to histological characteristics of invasive breast cancer. Polish J Pathol. 2016;3(3):295–299.

88. Lobbes MBI, Lalji UC, Nelemans PJ, et al. The Quality of Tumor Size Assessment by Contrast-Enhanced Spectral Mammography and the Benefit of Additional Breast MRI. J Cancer. 2015;6(2):144–150.

89. Blum KS, Rubbert C, Mathys B, Antoch G, Mohrmann S, Obenauer S. Use of contrast-enhanced spectral mammography for intramammary cancer staging. Acad Radiol. 2014;21(11):1363–1369.

90. Fallenberg EM, Dromain C, Diekmann F, et al. Contrast-enhanced spectral mammography versus MRI: Initial results in the detection of breast cancer and assessment of tumour size. Eur Radiol. 2014;24(1):256–264.

91. Ali-Mucheru M, Pockaj B, Patel B, et al. Contrast-enhanced digital mammography in the surgical management of breast cancer. Ann Surg Oncol. 2016;23(S5):649–655.

92. Patel BK, Ranjbar S, Wu T, et al. Computer-aided diagnosis of contrast-enhanced spectral

mammography: A feasibility study. Eur J Radiol. 2018;98:207–213.

93. Luczyńska E, Heinze-Paluchowska S, Dyczek S, Blecharz P, Rys J, Reinfuss M. Contrast-enhanced spectral mammography: comparison with conventional mammography and histopathology in 152 women. Korean J Radiol. 2014;15(6):689.

94. Luczynska E, Niemiec J, Heinze S, et al. Intensity and pattern of enhancement on CESM: prognostic significance and its relation to expression of podoplanin in tumor stroma - a preliminary report. Anticancer Res. 2018;38(2):1085–1095.

95. Iotti V, Ravaioli S, Vacondio R, et al. Contrast-enhanced spectral mammography in neoadjuvant chemotherapy monitoring: a comparison with breast magnetic resonance imaging. Breast Cancer Res. 2017;19(1):106.

96. Patel BK, Hilal T, Covington M, et al. Contrast-enhanced spectral mammography is comparable to MRI in the assessment of residual breast cancer following neoadjuvant systemic therapy. Ann Surg Oncol. 2018;25(5):1350–1356.

97. Barra FR, Souza FF de, Camelo REFA, Ribeiro AC de O, Farage L. Accuracy of contrast-enhanced spectral mammography for estimating residual tumor size after neoadjuvant chemotherapy in patients with breast cancer: a feasibility study. Radiol Bras. 2017;50(4):224–230.

98. Barra FR, Sobrinho AB, Barra RR, et al. Contrast-enhanced mammography (CEM) for detecting residual disease after neoadjuvant chemotherapy: a comparison with breast magnetic resonance imaging (MRI). Biomed Res Int. 2018;2018:1–9.

99. Tagliafico AS, Bignotti B, Rossi F, et al. Diagnostic performance of contrast-enhanced spectral mammography: Systematic review and meta-analysis. The Breast. 2016;28:13–19.

100. Zhu X, Huang J ming, Zhang K, et al. Diagnostic value of contrast-enhanced spectral mammography for screening breast cancer: systematic review and meta-analysis. Clin Breast Cancer. 2018;18(5):e985–e995.

101. Sardanelli F, Boetes C, Borisch B, et al. Magnetic resonance imaging of the breast:

Recommendations from the EUSOMA working group. Eur J Cancer. 2010;46(8):1296–1316.

102. Mann RM, Kuhl CK, Kinkel K, Boetes C. Breast MRI: guidelines from the European Society of Breast Imaging. Eur Radiol. 2008;18(7):1307–1318.

103. The American Society of Breast Surgeons. Consensus guideline on diagnostic and screening magnetic resonance imaging of the breast.

104. American College of Radiology. ACR practice parameter for the performance of contrast-enhanced magnetic resonance imaging (MRI) of the breast.

105. Zanardo M, Cozzi A, Trimboli RM, Carbonaro LA, Sardanelli F. Technique and diagnostic performance of contrast-enhanced spectral mammography: a systematic review. PROSPERO 2018 CRD42018118554.

106. Moher D, Liberati A, Tetzlaff J, Altman DG, PRISMA Group. Preferred Reporting Items for Systematic Reviews and Meta-Analyses: The PRISMA Statement. PLoS Med. 2009;6(7):e1000097.

107. Egger M, Davey Smith G, Schneider M, Minder C. Bias in meta-analysis detected by a simple, graphical test. BMJ. 1997;315(7109):629–634.

108. Luczyńska E, Heinze S, Adamczyk A, Rys J, Mitus JW, Hendrick E. Comparison of the mammography, contrast-enhanced spectral mammography and ultrasonography in a group of 116 patients. Anticancer Res. 2016;36(8):4359–4366.

109. Tohamey YM, Youssry SW, Abd El Aziz AI. Interpretation of patterns of enhancement on contrast-enhanced spectral mammography: an approach to a standardized scheme. Egypt J Radiol Nucl Med. 2018;49(3):854–868.

110. Dromain C, Thibault F, Diekmann F, et al. Dual-energy contrast-enhanced digital mammography: initial clinical results of a multireader, multicase study. Breast Cancer Res. 2012;14(3):R94.

111. Łuczyńska E, Heinze-Paluchowska S, Hendrick E, et al. Comparison between breast MRI and contrast-enhanced spectral mammography. Med Sci Monit. 2015;21(11):1358–1367.

112. Jochelson MS, Pinker K, Dershaw DD, et al. Comparison of screening CEDM and MRI for women at increased risk for breast cancer: A pilot study. Eur J Radiol. 2017;97(5):37–43.

113. Jochelson MS, Dershaw DD, Sung JS, et al. Bilateral contrast-enhanced dual-energy digital mammography: feasibility and comparison with conventional digital mammography and mr imaging in women with known breast carcinoma. Radiology. 2013;266(3):743–751.

114. James JR, Pavlicek W, Hanson JA, Boltz TF, Patel BK. Breast radiation dose with cesm compared with 2D FFDM and 3D tomosynthesis mammography. Am J Roentgenol. 2017;208(2):362–372.

115. Mokhtar O, Mahmoud S. Can contrast enhanced mammography solve the problem of dense breast lesions? Egypt J Radiol Nucl Med. 2014;45(3):1043–1052.

116. Houben IPL, Van de Voorde P, Jeukens CRLPN, et al. Contrast-enhanced spectral mammography as work-up tool in patients recalled from breast cancer screening has low risks and might hold clinical benefits. Eur J Radiol. 2017;94(March):31–37.

117. Dromain C, Thibault F, Muller S, et al. Dual-energy contrast-enhanced digital mammography: initial clinical results. Eur Radiol. 2011;21(3):565–574.

118. Jeukens CRLPN, Lalji UC, Meijer E, et al. Radiation exposure of contrast-enhanced spectral mammography compared with full-field digital mammography. Invest Radiol. 2014;49(10):659–665.

119. Diekmann F, Freyer M, Diekmann S, et al. Evaluation of contrast-enhanced digital mammography. Eur J Radiol. 2011;78(1):112–121.

120. Richter V, Hatterman V, Preibsch H, et al. Contrast-enhanced spectral mammography in patients with MRI contraindications. Acta radiol. 2018;59(7):798–805.

121. Lobbes MBII, Lalji U, Houwers J, et al. Contrast-enhanced spectral mammography in patients referred from the breast cancer screening programme. Eur Radiol. 2014;24(7):1668–1676.

122. Gluskin J, Click M, Fleischman R, Dromain C, Morris EA, Jochelson MS. Contamination

artifact that mimics in-situ carcinoma on contrast-enhanced digital mammography. Eur J Radiol. 2017;95:147–154.

123. Travieso Aja MM, Rodríguez Rodríguez M, Alayón Hernández S, Vega Benítez V, Luzardo OP. Mamografía con realce de contraste mediante técnica de energía dual. Radiologia. 2014;56(5):390–399.

124. Patel BK, Naylor ME, Kosiorek HE, et al. Clinical utility of contrast-enhanced spectral mammography as an adjunct for tomosynthesis-detected architectural distortion. Clin Imaging. 2017;46:44–52.

125. Francescone MA, Jochelson MS, Dershaw DD, et al. Low energy mammogram obtained in contrast-enhanced digital mammography (CEDM) is comparable to routine full-field digital mammography (FFDM). Eur J Radiol. 2014;83(8):1350–1355.

126. Łuczyńska E, Niemiec J, Hendrick E, et al. Degree of enhancement on contrast enhanced spectral mammography (CESM) and lesion type on mammography (MG): comparison based on histological results. Med Sci Monit. 2016;22:3886–3893.

127. Kariyappa KD, Gnanaprakasam F, Anand S, Krishnaswami M, Ramachandran M. Contrast enhanced dual energy spectral mammogram, an emerging addendum in breast imaging. Br J Radiol. 2016;89(1067).

128. Danala G, Patel B, Aghaei F, et al. Classification of breast masses using a computer-aided diagnosis scheme of contrast enhanced digital mammograms. Ann Biomed Eng. 2018;46(9):1419–1431.

129. Phillips J, Miller MM, Mehta TS, et al. Contrast-enhanced spectral mammography (CESM) versus MRI in the high-risk screening setting: patient preferences and attitudes. Clin Imaging. 2017;42:193–197.

130. Yagil Y, Shalmon A, Rundstein A, et al. Challenges in contrast-enhanced spectral mammography interpretation: artefacts lexicon. Clin Radiol. 2016;71(5):450–457.

131. Cheung Y-C, Tsai H-P, Lo Y-F, Ueng S-H, Huang P-C, Chen S-C. Clinical utility of dual-

energy contrast-enhanced spectral mammography for breast microcalcifications without associated mass: a preliminary analysis. Eur Radiol. 2016;26(4):1082–1089.

132. ElSaid NAE, Farouk S, Shetat OMM, Khalifa NM, Nada OM. Contrast enhanced digital mammography: Is it useful in detecting lesions in edematous breast? Egypt J Radiol Nucl Med. 2015;46(3):811–819.

133. Mori M, Akashi-Tanaka S, Suzuki S, et al. Diagnostic accuracy of contrast-enhanced spectral mammography in comparison to conventional full-field digital mammography in a population of women with dense breasts. Breast Cancer. 2017;24(1):104–110.

134. Savaridas SL, Taylor DB, Gunawardana D, Phillips M. Could parenchymal enhancement on contrast-enhanced spectral mammography (CESM) represent a new breast cancer risk factor? Correlation with known radiology risk factors. Clin Radiol. 2017;72(12):1085.e1-1085.e9.

135. Fallenberg EM, Schmitzberger FF, Amer H, et al. Contrast-enhanced spectral mammography vs. mammography and MRI – clinical performance in a multi-reader evaluation. Eur Radiol. 2017;27(7):2752–2764.

136. Brandan M-E, Cruz-Bastida JP, Rosado-Méndez IM, et al. Clinical study of contrast-enhanced digital mammography and the evaluation of blood and lymphatic microvessel density. Br J Radiol. 2016;89(1065).

137. Lalji UC, Houben IPLL, Prevos R, et al. Contrast-enhanced spectral mammography in recalls from the Dutch breast cancer screening program: validation of results in a large multireader, multicase study. Eur Radiol. 2016;26(12):4371–4379.

138. Deng C-Y, Juan Y-H, Cheung Y-C, et al. Quantitative analysis of enhanced malignant and benign lesions on contrast-enhanced spectral mammography. Br J Radiol. 2018;91(1086).

139. Mohamed Kamal R, Hussien Helal M, Wessam R, Mahmoud Mansour S, Godda I, Alieldin N. Contrast-enhanced spectral mammography: Impact of the qualitative morphology descriptors on the diagnosis of breast lesions. Eur J Radiol. 2015;84(6):1049–1055.

140. Sogani J, Morris EA, Kaplan JB, et al. Comparison of background parenchymal enhancement

at contrast-enhanced spectral mammography and breast MR imaging. Radiology. 2017;282(1):63–73.

141. Hobbs MM, Taylor DB, Buzynski S, Peake RE. Contrast-enhanced spectral mammography (CESM) and contrast enhanced MRI (CEMRI): Patient preferences and tolerance. J Med Imaging Radiat Oncol. 2015;59(3):300–305.

142. Phillips J, Mihai G, Hassonjee SE, et al. Comparative dose of contrast-enhanced spectral mammography (CESM), digital mammography, and digital breast tomosynthesis. Am J Roentgenol. 2018;211(4):839–846.

143. Knogler T, Homolka P, Hörnig M, et al. Contrast-enhanced dual energy mammography with a novel anode/filter combination and artifact reduction: a feasibility study. Eur Radiol. 2016;26(6):1575–1581.

144. Xing D, Lv Y, Sun B, et al. Diagnostic value of contrast-enhanced spectral mammography in comparison to magnetic resonance imaging in breast lesions. J Comput Assist Tomogr. 2018;

145. Fallenberg EM, Dromain C, Diekmann F, et al. Contrast-enhanced spectral mammography: Does mammography provide additional clinical benefits or can some radiation exposure be avoided? Breast Cancer Res Treat. 2014;146(2):371–381.

146. Cheung Y-C, Lin Y-C, Wan Y-L, et al. Diagnostic performance of dual-energy contrast-enhanced subtracted mammography in dense breasts compared to mammography alone: interobserver blind-reading analysis. Eur Radiol. 2014;24(10):2394–2403.

147. Kim EY, Youn I, Lee KH, et al. Diagnostic value of contrast-enhanced digital mammography versus contrast-enhanced magnetic resonance imaging for the preoperative evaluation of breast cancer. J Breast Cancer. 2018;21(4):453.

148. Klang E, Krosser A, Amitai MM, et al. Utility of routine use of breast ultrasound following contrast-enhanced spectral mammography. Clin Radiol. 2018;73(10).

149. Tsigginou A, Gkali C, Chalazonitis A, et al. Adding the power of iodinated contrast media to the credibility of mammography in breast cancer diagnosis. Br J Radiol. 2016;89(1067).

150. Navarro ME, Razmilic D, Araos I, Rodrigo A, Andia ME. Rendimiento de la mamografía espectral de energía dual con contraste en la detección de cáncer de mama: experiencia en un centro de referencia. Rev Med Chil. 2018;146(2):141–149.

151. Luczynska E, Niemiec J, Ambicka A, et al. Correlation between blood and lymphatic vessel density and results of contrast-enhanced spectral mammography. Polish J Pathol. 2015;3(3):310–322.

152. Sorin V, Yagil Y, Yosepovich A, et al. Contrast-enhanced spectral mammography in women with intermediate breast cancer risk and dense breasts. Am J Roentgenol. 2018;211(5):W267–W274.

153. Bicchierai G, Nori J, De Benedetto D, et al. Role of contrast-enhanced spectral mammography in the post biopsy management of B3 lesions: Preliminary results. Tumori J. 2018;

154. Knogler T, Homolka P, Hoernig M, et al. Application of BI-RADS descriptors in contrast-enhanced dual-energy mammography: comparison with MRI. Breast Care. 2017;12(4):212–216.

155. Kamal RM, Helal MH, Mansour SM, et al. Can we apply the MRI BI-RADS lexicon morphology descriptors on contrast-enhanced spectral mammography? Br J Radiol. 2016;89(1064).

156. Lewin JM, Isaacs PK, Vance V, Larke FJ. Dual-energy contrast-enhanced digital subtraction mammography: feasibility. Radiology. 2003;229(1):261–268.

157. Wang Q, Li K, Wang L, Zhang J, Zhou Z, Feng Y. Preclinical study of diagnostic performances of contrast-enhanced spectral mammography versus MRI for breast diseases in China. Springerplus. 2016;5(1):763.

158. Cheung Y-C, Juan Y-H, Lin Y-C, et al. Dual-energy contrast-enhanced spectral mammography: enhancement analysis on BI-RADS 4 non-mass microcalcifications in screened women. PLoS One. 2016;11(9).

159. Helal M, Abu Samra MF, Ibraheem MA, Salama A, Hassan EE, Hassan NE-HH. Accuracy of CESM versus conventional mammography and ultrasound in evaluation of BI-RADS 3 and 4 breast lesions with pathological correlation. Egypt J Radiol Nucl Med. 2017;48(3):741–750.

160. Li L, Roth R, Germaine P, et al. Contrast-enhanced spectral mammography (CESM) versus breast magnetic resonance imaging (MRI): A retrospective comparison in 66 breast lesions. Diagn Interv Imaging. 2017;98(2):113–123.

161. Badr S, Laurent N, Régis C, Boulanger L, Lemaille S, Poncelet E. Dual-energy contrast-enhanced digital mammography in routine clinical practice in 2013. Diagn Interv Imaging. 2014;95(3):245–258.

162. Houben IP, Vanwetswinkel S, Kalia V, et al. Contrast-enhanced spectral mammography in the evaluation of breast suspicious calcifications: diagnostic accuracy and impact on surgical management. Acta radiol. 2019;

163. Covington MF, Pizzitola VJ, Lorans R, et al. The future of contrast-enhanced mammography. Am J Roentgenol. 2018;210(2):292–300.

164. Lancaster RB, Gulla S, De Los Santos J, Umphrey HR. Contrast-enhanced spectral mammography in breast imaging. Semin Roentgenol. 2018;53(4):294–300.

165. James JJ, Tennant SL. Contrast-enhanced spectral mammography (CESM). Clin Radiol. 2018;73(8):715–723.

166. Patel BK, Gray RJ, Pockaj BA. Potential cost savings of contrast-enhanced digital mammography. Am J Roentgenol. 2017;208(6):W231–W237.

167. Minsinger KD, Kassis HM, Block CA, Sidhu M, Brown JR. Meta-analysis of the effect of automated contrast injection devices versus manual injection and contrast volume on risk of contrast-induced nephropathy. Am J Cardiol. 2014;113(1):49–53.

168. Endrikat J, Barbati R, Scarpa M, Jost G, (Ned) Uber AE. Accuracy and repeatability of automated injector versus manual administration of an mri contrast agent—results of a

laboratory study. Invest Radiol. 2018;53(1):1–5.

169. Jost G, Endrikat J, Pietsch H. The impact of injector-based contrast agent administration on bolus shape and magnetic resonance angiography image quality. Magn Reson Insights. 2017;10:1178623X1770589.

170. Auler MA, Heagy T, Aganovic L, Brothers R, Costello P, Schoepf UJ. Saline chasing technique with dual-syringe injector systems for multi-detector row computed tomographic angiography: rationale, indications, and protocols. Curr Probl Diagn Radiol. 2006;35(1):1–11.

171. Kidoh M, Nakaura T, Awai K, et al. Novel connecting tube for saline chaser in contrast-enhanced CT: the effect of spiral flow of saline on contrast enhancement. Eur Radiol. 2013;23(11):3213–3218.

172. Perry N, Broeders M, de Wolf C, Tornberg S, Holland R, von Karsa L. European guidelines for quality assurance in breast cancer screening and diagnosis. Fourth edition--summary document. Ann Oncol. 2007;19(4):614–622.

173. Wang CL, Cohan RH, Ellis JH, Caoili EM, Wang G, Francis IR. Frequency, outcome, and appropriateness of treatment of nonionic iodinated contrast media reactions. Am J Roentgenol. 2008;191(2):409–415.

174. Mortelé KJ, Oliva M-R, Ondategui S, Ros PR, Silverman SG. Universal use of nonionic iodinated contrast medium for CT: evaluation of safety in a large urban teaching hospital. Am J Roentgenol. 2005;184(1):31–34.

175. Huston P, Moher D. Redundancy, disaggregation, and the integrity of medical research. Lancet (London, England). 1996;347(9007):1024–1026.

176. Murphy L, Wyllie A. Duplicate patient data in a meta-analysis; a threat to validity. J Crit Care. 2009;24(3):466–467.

177. Sardanelli F, Alì M, Hunink MG, Houssami N, Sconfienza LM, Di Leo G. To share or not to share? Expected pros and cons of data sharing in radiological research. Eur Radiol.

2018;28(6):2328–2335.

178. Rogosnitzky M, Branch S. Gadolinium-based contrast agent toxicity: a review of known and proposed mechanisms. BioMetals. June 2016;1–12.

179. White GW, Gibby WA, Tweedle MF. Comparison of Gd (DTPA-BMA) (Omniscan) versus retention in human bone tissue by inductively coupled plasma mass spectroscopy. Invest Radiol. 2006;41(3):272–278.

180. Kanda T, Ishii K, Kawaguchi H, Kitajima K, Takenaka D. High signal intensity in the dentate nucleus and globus pallidus on unenhanced T1-weighted MR images: relationship with increasing cumulative dose of a gadolinium-based contrast material. Radiology. 2014;270(3):834–841.

181. Errante Y, Cirimele V, Mallio CA, Di Lazzaro V, Zobel BB, Quattrocchi CC. Progressive increase of T1 signal intensity of the dentate nucleus on unenhanced magnetic resonance images is associated with cumulative doses of intravenously administered gadodiamide in patients with normal renal function, suggesting dechelation. Invest Radiol. 2014;00(00):1–6.

182. Quattrocchi CC, Ad- MGC. High T1 Signal intensity in dentate nucleus after multiple injections of linear gadolinium chelates. Radiology. 2015;276(2):616–617.

183. Radbruch A, Weberling LD., Kieslich PJ, et al. Gadolinium retention in the dentate nucleus and globus pallidus is dependent on the class of contrast agent. Radiology. 2015;275(3):150337.

184. Stojanov DA, Aracki-Trenkic A, Vojinovic S, Benedeto-Stojanov D, Ljubisavljevic S. Increasing signal intensity within the dentate nucleus and globus pallidus on unenhanced T1W magnetic resonance images in patients with relapsing-remitting multiple sclerosis: correlation with cumulative dose of a macrocyclic gadolinium-based contrast age. Eur Radiol. 2016;26(3):807–815.

185. Weberling LD. Increased signal intensity in the dentate nucleus on unenhanced T1-weighted images after gadobenate dimeglumine administration. Invest Radiol. 2015;50(3):743–748.

186. Ramalho J, Ramalho M, AlObaidy M, Nunes RH, Castillo M, Semelka RC. T1 Signal-intensity increase in the dentate nucleus after multiple exposures to gadodiamide: intraindividual comparison between 2 commonly used sequences. AJNR Am J Neuroradiol. 2016;

187. Adin ME, Kleinberg L, Vaidya D, Zan E, Mirbagheri XS, Yousem XDM. Hyperintense dentate nuclei on T1-weighted MRI: relation to repeat gadolinium administration. Am J Neuroradiol. 2015;36(10):1859–1865.

188. Hirano S, Suzuki KT. Exposure, metabolism, and toxicity of rare earths and related compounds. Environ Health Perspect. 1996;104 Suppl:85–95.

189. Port M, Idée J-M, Medina C, Robic C, Sabatou M, Corot C. Efficiency, thermodynamic and kinetic stability of marketed gadolinium chelates and their possible clinical consequences: a critical review. Biometals. 2008;21(4):469–490.

190. Murata N, Gonzalez-Cuyar LF, Murata K, et al. Macrocyclic and other non-group 1 gadolinium contrast agents deposit low levels of gadolinium in brain and bone tissue: preliminary results from 9 patients with normal renal function. Invest Radiol. 2016;51(7):447–453.

191. McDonald RJ, McDonald JS, Kallmes DF, et al. Intracranial gadolinium deposition after contrast-enhanced MR imaging. Radiology. 2015;(3).

192. Vogt FM, Theysohn JM, Michna D, et al. Contrast-enhanced time-resolved 4D MRA of congenital heart and vessel anomalies: image quality and diagnostic value compared with 3D MRA. Eur Radiol. 2013;23(9):2392–2404.

193. Zghaib T, Shahid A, Pozzessere C, et al. Validation of contrast-enhanced time-resolved magnetic resonance angiography in pre-ablation planning in patients with atrial fibrillation: comparison with traditional technique. Int J Cardiovasc Imaging. 2018;34(9):1451–1458.

194. TRICKS / TWIST - Questions and Answers in MRI.

195. Muscogiuri G, Suranyi P, Eid M, et al. Pediatric Cardiac MR imaging: practical preoperative

assessment. Magn Reson Imaging Clin N Am. 2019;27(2):243–262.

196. Gaydos SS, Varga-Szemes A, Judd RN, Suranyi P, Gregg D. Imaging in adult congenital heart disease. J Thorac Imaging. 2017;32(4):205–216.

197. De Cecco CN, Muscogiuri G, Madrid Pérez JM, et al. Pictorial review of surgical anatomy in adult congenital heart disease. J Thorac Imaging. 2017;32(4):217–232.

198. Muscogiuri G, Secinaro A, Ciliberti P, Fuqua M, Nutting A. Utility of cardiac magnetic resonance imaging in the management of adult congenital heart disease. J Thorac Imaging. 2017;32(4):233–244.

199. Asaduddin M, Do W-J, Kim EY, Park S-H. Mapping cerebral perfusion from time-resolved contrast-enhanced MR angiographic data. Magn Reson Imaging. 2019;61:143–148.

200. Roh HG, Kim EY, Kim IS, et al. A novel collateral imaging method derived from time-resolved dynamic contrast-enhanced MR angiography in acute ischemic stroke: a pilot study. Am J Neuroradiol. 2019;

201. Shin JH, Choi Y, Park B, et al. Diagnostic accuracy and efficiency of combined acquisition of low-dose time-resolved and single-phase high-resolution contrast-enhanced magnetic resonance angiography in a single session for pre-angiographic evaluation of spinal vascular disease. PLoS One. 2019;14(3):e0214289.

202. Bak SH, Roh HG, Moon W-J, Choi JW, An HS. Appropriate minimal dose of gadobutrol for 3D Time-Resolved MRA of the supra-aortic arteries: comparison with conventional single-phase high-resolution 3D Contrast-enhanced MRA. Am J Neuroradiol. 2017;38(7):1383–1390.

203. Cui H, Yan R, Zhai Z, et al. Comparative analysis of 3D time-resolved contrast-enhanced magnetic resonance angiography, color Doppler ultrasound and digital subtraction angiography in symptomatic carotid stenosis. Exp Ther Med. 2017;15(2):1654–1659.

204. Le Y, Kipfer H, Majidi S, et al. Application of time-resolved angiography with stochastic trajectories (twist)-dixon in dynamic contrast-enhanced (dce) breast mri. J Magn Reson

Imaging. 2013;38(5):1033–1042.

205. Schicchi N, Tagliati C, Agliata G, Esposto Pirani P, Spadari R, Giovagnoni A. MRI evaluation of peripheral vascular anomalies using time-resolved imaging of contrast kinetics (TRICKS) sequence. Radiol Med. 2018;123(8):563–571.

206. Jin T, Wu G, Li X, Feng X. Evaluation of vascular invasion in patients with musculoskeletal tumors of lower extremities: use of time-resolved 3D MR angiography at 3-T. Acta radiol. 2018;59(5):586–592.

207. Armstrong L, Rodrigues JCL, Lawton CB, Tyrell-Price J, Hamilton MCK, Manghat NE. Application of TWIST MR angiography to aid successful central venous access in challenging patients: initial single-centre experience. Clin Radiol. 2016;71(11):1104–1112.

208. Lee JJ, Tirman PJ, Chang Y, et al. The optimization of scan timing for contrast-enhanced magnetic resonance angiography. Korean J Radiol. 2000;1(3):142–151.

209. Menke J. Carotid MR angiography with traditional bolus timing: clinical observations and Fourier-based modelling of contrast kinetics. Eur Radiol. 2009;19(11):2654–2662.

210. Medicines Agency E. PRAC concludes assessment of gadolinium agents used in body scans and recommends regulatory actions, including suspension for some marketing authorisations. 2017.

211. Hadizadeh DR, Keil VC, Jost G, et al. Contrast media in Time-Resolved MRA at 3T: a systematic quantitative and qualitative analysis of concentration and dose effects on image parameters in minipigs. RoFo Fortschritte auf dem Gebiet der Rontgenstrahlen und der Bildgeb Verfahren. 2018;190(8):747–757.

212. Runge VM. Critical questions regarding gadolinium deposition in the brain and body after injections of the gadolinium-based contrast agents, safety, and clinical recommendations in consideration of the EMA's pharmacovigilance and risk assessment committee recommendation for suspension of the marketing authorizations for 4 linear agents. Invest Radiol. 2017;52(6):317–323.

213. Hennig J, Scheffler K, Laubenberger J, Strecker R. Time-resolved projection angiography after bolus injection of contrast agent. Magn Reson Med. 1997;37(3):341–345.

214. Goo HW, Yang DH, Park I-S, et al. Time-resolved three-dimensional contrast-enhanced magnetic resonance angiography in patients who have undergone a Fontan operation or bidirectional cavopulmonary connection: Initial experience. J Magn Reson Imaging. 2007;25(4):727–736.

215. Nael K, Krishnam M, Ruehm SG, Michaely HJ, Laub G, Finn JP. Time-Resolved MR angiography in the evaluation of central thoracic venous occlusive disease. Am J Roentgenol. 2009;192(6):1731–1738.

216. Seng K, Maderwald S, de Greiff A, et al. Dynamic contrast-enhanced magnetic resonance angiography of the thoracic vessels. Invest Radiol. 2010;45(11):708–714.

217. Faggioni L, Zampa V, Ortori S, et al. Time-resolved contrast-enhanced magnetic resonance angiography (CEMRA) of the left atrium-pulmonary veins complex with half dose of intravenous gadolinium-based contrast agent. Technical feasibility and comparison with a conventional CEMRA, full contrast . Eur J Radiol. 2012;81(2):250–256.

218. Speiser U, Tränkner A, Kappert U, Sievers B, Strasser R, Schön S. Feasibility of time resolved magnetic resonance imaging of contrast kinetics to identify severe tricuspid valve regurgitation. RöFo - Fortschritte auf dem Gebiet der Röntgenstrahlen und der Bildgeb Verfahren. 2010;182(02).

219. Rapacchi S, Han F, Natsuaki Y, et al. High spatial and temporal resolution dynamic contrast-enhanced magnetic resonance angiography using compressed sensing with magnitude image subtraction. Magn Reson Med. 2014;71(5):1771–1783.

220. Rapacchi S, Natsuaki Y, Plotnik A, et al. Reducing view-sharing using compressed sensing in time-resolved contrast-enhanced magnetic resonance angiography. Magn Reson Med. 2015;74(2):474–481.

221. Rustogi R, Galizia M, Thakrar D, et al. Steady-state MRA techniques with a blood pool

contrast agent improve visualization of pulmonary venous anatomy and left atrial patency compared with time-resolved MRA pre- and postcatheter ablation in atrial fibrillation. J Magn Reson Imaging. 2015;42(5):1305–1313.

222. Wetzl J, Forman C, Wintersperger BJ, et al. High-resolution dynamic CE-MRA of the thorax enabled by iterative TWIST reconstruction. Magn Reson Med. 2017;77(2):833–840.

223. Obara-Moszynska M, Rajewska-Tabor J, Rozmiarek S, et al. The usefulness of magnetic resonance imaging of the Cardiovascular system in the diagnostic work-up of patients with Turner syndrome. Front Endocrinol (Lausanne). 2018;9(OCT):1–10.

224. Sugrue G, Cradock A, McGee A, et al. Subtraction of time-resolved magnetic resonance angiography images improves visualization of the pulmonary veins and left atrium in adults with congenital heart disease: a novel post-processing technique. Int J Cardiovasc Imaging. 2019;(0123456789).

225. Krishnam MS, Tomasian A, Lohan DG, Tran L, Finn JP, Ruehm SG. Low-dose, time-resolved, contrast-enhanced 3D MR angiography in cardiac and vascular diseases: correlation to high spatial resolution 3D contrast-enhanced MRA. Clin Radiol. 2008;63(7):744–755.

226. van Vaals JJ, Brummer ME, Dixon WT, et al. “Keyhole” method for accelerating imaging of contrast agent uptake. J Magn Reson Imaging. 3(4):671–675.

227. Jones RA, Haraldseth O, Müller TB, Rinck PA, Oksendal AN. K-space substitution: a novel dynamic imaging technique. Magn Reson Med. 1993;29(6):830–834.

228. Hadizadeh D, Marx C, Gieseke J, Schild H, Willinek W. High temporal and high spatial resolution MR angiography (4D-MRA). RöFo - Fortschritte auf dem Gebiet der Röntgenstrahlen und der Bildgeb Verfahren. 2014;186(09):847–859.

229. Young PM, McGee KP, Pieper MS, et al. Tips and tricks for MR angiography of pediatric and adult congenital cardiovascular diseases. Am J Roentgenol. 2013;200(5):980–988.

230. Lim RP, Koktzoglou I. Noncontrast Magnetic Resonance Angiography. Radiol Clin North

Am. 2015;53(3):457–476.

231. Constantinides C. Protocols and methodologies in basic science and clinical cardiac MRI. 2018.

232. Campeau NG, Huston J, Bernstein MA, Lin C, Gibbs GF. Magnetic Resonance Angiography at 3.0 Tesla: Initial Clinical Experience. Top Magn Reson Imaging. 2001;12(3):183–204.

233. Willinek WA, Born M, Simon B, et al. Time-of-Flight MR Angiography: Comparison of 3.0-T Imaging and 1.5-T Imaging—Initial Experience. Radiology. 2003;229(3):913–920.

234. The Royal College of Radiologists. Guidance on gadolinium-based contrast agent administration to adult patients. .

235. Bhave G, Lewis JB, Chang SS. Association of Gadolinium Based MRI Contrast Agents and Nephrogenic Systemic Fibrosis. J Urol. 2008;180(3):830.

236. Thomsen HS, European Society of Urogenital Radiology (ESUR). ESUR guideline: gadolinium-based contrast media and nephrogenic systemic fibrosis. Eur Radiol. 2007;17(10):2692–2696.

237. Thomsen HS, Morcos SK, Almén T, et al. ESUR Guidelines on Contrast Media. 2009. p. 229–242.

238. Rohrer M, Bauer H, Mintorovitch J, Requardt M, Weinmann H-J. Comparison of Magnetic Properties of MRI Contrast Media Solutions at Different Magnetic Field Strengths. Invest Radiol. 2005.

239. Szomolanyi P, Rohrer M, Frenzel T, et al. Comparison of the Relaxivities of Macrocyclic Gadolinium-Based Contrast Agents in Human Plasma at 1.5, 3, and 7 T, and Blood at 3 T. Invest Radiol. 2019;1.

240. Pintaske J, Martirosian P, Graf H, et al. Relaxivity of Gadopentetate Dimeglumine (Magnevist), Gadobutrol (Gadovist), and Gadobenate Dimeglumine (MultiHance) in Human Blood Plasma at 0.2, 1.5, and 3 Tesla. Invest Radiol. 2006;41(3):213–221.

241. Wildgruber M, Stadlbauer T, Rasper M, et al. Single-dose gadobutrol in comparison with

single-dose gadobenate dimeglumine for magnetic resonance imaging of chronic myocardial infarction at 3 T. Invest Radiol. 2014;49(11):728–734.

242. Gulani V, Calamante F, Shellock FG, Kanal E, Reeder SB. Gadolinium deposition in the brain: summary of evidence and recommendations. Lancet Neurol. 2017;16(7):564–570.

243. Guo BJ, Yang ZL, Zhang LJ. Gadolinium Deposition in Brain: Current Scientific Evidence and Future Perspectives. Front Mol Neurosci. 2018;11.

244. Costa AF, van der Pol CB, Maralani PJ, et al. Gadolinium deposition in the brain: a systematic review of existing guidelines and policy statement issued by the Canadian association of radiologists. Can Assoc Radiol J. 2018;69(4):373–382.

245. Tombach B, Heindel W. Value of 1.0-M gadolinium chelates: review of preclinical and clinical data on gadobutrol. Eur Radiol. 2002;12(6):1550–1556.

246. Giesel FL, Mehndiratta A, Essig M. High-relaxivity contrast-enhanced magnetic resonance neuroimaging: a review. Eur Radiol. 2010;20(10):2461–2474.

247. Frydrychowicz A, Russe MF, Bock J, et al. Comparison of Gadofosveset Trisodium and Gadobenate Dimeglumine During Time-Resolved Thoracic MR Angiography at 3T. Acad Radiol. 2010;17(11):1394–1400.

248. Hadizadeh DR, Jost G, Pietsch H, et al. Intraindividual quantitative and qualitative comparison of gadopentetate dimeglumine and gadobutrol in time-resolved contrast-enhanced 4-dimensional magnetic resonance angiography in minipigs. Invest Radiol. 2014;49(7):457–464.

249. Budjan J, Ong M, Riffel P, et al. CAIPIRINHA-Dixon-TWIST (CDT)-volume-interpolated breath-hold examination (VIBE) for dynamic liver imaging: Comparison of gadoterate meglumine, gadobutrol and gadoxetic acid. Eur J Radiol. 2014;83(11):2007–2012.

250. Ai T, Goerner F, Patel N, et al. Contrast dose, temporal footprint, and spatial resolution tradeoffs in dynamic contrast-enhanced MRA performed in a porcine model of a carotid aneurysm. J Comput Assist Tomogr. 2013;37(1):105–110.

251. Jourdan C, Heverhagen JT, Knopp MV. Dose comparison of single- vs. double-dose in contrast-enhanced magnetic resonance angiography of the carotid arteries: Intraindividual cross-over blinded trial using Gd-DTPA. J Magn Reson Imaging. 2007;25(3):557–563.

252. Böhm I, Morelli J, Nairz K, Silva Hasembank Keller P, Heverhagen JT. Myths and misconceptions concerning contrast media-induced anaphylaxis: a narrative review. Postgrad Med. 2017;129(2):259–266.

253. Riederer SJ, Haider CR, Borisch EA, Weavers PT, Young PM. Recent advances in 3D time-resolved contrast-enhanced MR angiography. J Magn Reson Imaging. 2015;42(1):3–22.

254. Barth M, Poser BA. Advances in High-Field BOLD fMRI. Mater (Basel, Switzerland). 2011;4(11):1941–1955.

255. Bojorquez JZ, Bricq S, Acquitter C, Brunotte F, Walker PM, Lalande A. What are normal relaxation times of tissues at 3 T? Magn Reson Imaging. 2017;35:69–80.

256. Budjan J, Attenberger UI, Schoenberg SO, Pietsch H, Jost G. The impact of injector-based contrast agent administration in time-resolved MRA. Eur Radiol. 2018;28(5):2246–2253.

Publications

1. Papini GDE, Di Leo G, Zanardo M, Fedeli MP, Merli I, Sardanelli F. Measurement of jugular foramen diameter using MRI in multiple sclerosis patients compared to control subjects. Eur Radiol Exp. 2017;1(1):4. doi: 10.1186/s41747-017-0008-3.
2. Secchi F, Di Leo G, Zanardo M, Alì M, Cannaò PM, Sardanelli F. Detection of incidental cardiac findings in noncardiac chest computed tomography. Medicine. 2017;96(29):e7531. doi: 10.1097/MD.0000000000007531.
3. Di Leo G, Spadavecchia C, Zanardo M, Secchi F, Veronese I, Cantone MC, Sardanelli F. Should the automatic exposure control system of CT be disabled when scanning patients with endoaortic stents or mechanical heart valves? A phantom study. Eur Radiol. 2017;27(7):2989-2994.
4. Doniselli FM, Zanardo M, Manfrè L, Papini GDE, Rovira A, Sardanelli F, Sconfienza LM, Arana E. A critical appraisal of the quality of low back pain practice guidelines using the AGREE II tool and comparison with previous evaluations: a EuroAIM initiative. Eur Spine J. 2018 Nov;27(11):2781-2790. Doi: 10.1007/s00586-018-5763-1
5. Zanardo M, Doniselli FM, Esseridou A, Tritella S, Mattiuz C, Menicagli L, Di Leo G, Sardanelli F. Abdominal CT: a radiologist-driven adjustment of the dose of iodinated contrast agent approaches a calculation per lean body weight. Eur Radiol Exp. 2018 Dec 5;2(1):41. Doi: 10.1186/s41747-018-0074-1
6. Sardanelli F, Schiaffino S, Zanardo M, Secchi F, Cannaò PM, Ambrogi F, Di Leo G. Point estimate and reference normality interval of MRI-derived myocardial extracellular volume in healthy subjects: a systematic review and meta-analysis. Eur Radiol. 2019. Doi: 10.1007/s00330-019-06185-w.
7. Zanardo M, Cozzi A, Trimboli RM, Labaj O, Monti CB, Schiaffino S, Carbonaro LA, Sardanelli F. Technique, protocols, and adverse reactions for contrast-enhanced spectral

mammography (CESM): a systematic review. Insight into Imaging. Doi: 10.1186/s13244-019-0756-0

8. Codari M, Zanardo M, di Sabato ME, Nocerino E, Messina C, Sconfienza LM, Sardanelli F. MRI-based quantitative assessment of sarcopenia: a systematic review. J Magn Reson Imaging. Doi: 10.1002/jmri.26931

Reviewer activities

1. European Journal of Radiology – Impact Factor: 2.948
2. Spine – Impact Factor: 2.792
3. European Radiology Experimental
4. Radiography

Reviews verified on Publons: https://publons.com/researcher/1485728/moreno-zanardo/

H-Index: 2

Scopus Author ID: 57192305462

OrcID: 0000-0001-9640-8534

Web of Science ResearcherID: J-3223-2019

Research Gate: Moreno_Zanardo | RG Score 16.32

PhD Fellowship

University College Dublin, Dublin, Ireland.

Mater Misericordiae University Hospital, Radiology department. Dublin, Ireland.

March 2019 – September 2019.

Advisor Prof. L. Rainford.

Acknowledgement

First and foremost, I would like to thank Prof. Francesco Sardanelli who have been more than my PhD tutor during these three years supporting me in research activities, for his patience, motivation and for inspiring me every single day.

My sincere thanks also goes to Prof. Louise Rainford who provided me with an opportunity to join her team as PhD fellow at University College Dublin, and who gave me access to the didactic and research facilities. Without her precious support it would have not been possible to live that amazing experience. I will always have a wonderful memory of all the moments spent in Ireland.

Besides my PhD advisor, I would like to thank the rest of Policlinico San Donato research team, more than "only" colleagues. The research group has been a source of friendships as well as good advice and collaboration. I thank my research mates for the stimulating discussions, the sleepless nights we worked together before deadlines, and for all the fun (& congresses) we have had in the last three years.

A special thanks goes to Maestro Kayoko Shuto, who taught me discipline, hard work and passion, since I was six years old. I will never stop thanking her for helping me to achieve the piano diploma during these intense years.

Last (but not the least), I would like to thank Sara and my family: my parents, my sister, my uncle and all my grandparents for supporting me spiritually throughout writing this thesis and my life in general. I am also grateful to my friends who have been great supporter along the way. These *"Ricerchine"* would not be possible without you.

Many thanks,

Moreno